nature reviews physics

https://doi.org/10.1038/s42254-023-00671-3

Review article

Check for updates

The physics of 3D printing with light

Paul Somers[1], Alexander Münchinger[2], Shoji Maruo[3,4,5], Christophe Moser[6], Xianfan Xu[7,8] & Martin Wegener[1,2]

Abstract

The goal of 3D printing is to realize complex 3D structures by locally adding material in small volume elements called voxels — in contrast to successively subtracting material by etching, milling or machining. This field started with optics-based proposals in the 1970s. Progress has required breakthroughs in physics, chemistry, materials science, laser science and engineering. This Review focuses on the physics underlying optics-based approaches, including interference lithography, tomographic volumetric additive manufacturing, stereolithography, continuous liquid-interface printing, light-sheet printing, parallelized spatiotemporal focusing and (multi-)focus scanning. Light–matter interactions that are discussed include one-photon, two-photon, multi-photon or cascaded nonlinear optical absorption processes for excitation and stimulated-emission depletion or excited-state absorption followed by reverse intersystem crossing for de-excitation. The future physics challenges lie in further boosting three metrics: spatial resolution, rate of voxel creation and range of available dissimilar material properties. Engineering challenges lie in achieving these metrics in compact, low-cost and low-energy-consumption instruments and in identifying new applications.

Sections

[1]Institute of Nanotechnology, Karlsruhe Institute of Technology, Karlsruhe, Germany. [2]Institute of Applied Physics, Karlsruhe Institute of Technology, Karlsruhe, Germany. [3]Faculty of Engineering, College of Engineering Sciences, Yokohama National University, Yokohama, Japan. [4]Institute of Advanced Sciences, Yokohama National University, Yokohama, Japan. [5]Institute for Multidisciplinary Sciences, Yokohama National University, Yokohama, Japan. [6]Laboratory of Applied Photonics Devices, École Polytechnique Fédérale Lausanne, Lausanne, Switzerland. [7]School of Mechanical Engineering, Purdue University, West Lafayette, IN, USA. [8]Birck Nanotechnology Center, Purdue University, West Lafayette, IN, USA. e-mail: martin.wegener@kit.edu

Key points

- Three-dimensional printing with light is an additive manufacturing process in which light irradiation locally adds a solid material (typically from a liquid 'ink'), rather than subtracting it from a solid by machining or drilling, to form complex 3D structures from the macroscale to the nanoscale.
- All current light-based 3D printing modalities (including interference lithography, spatial focusing, spatiotemporal focusing, tomographic volumetric additive manufacturing and layer-by-layer approaches) can be seen as approximations of an ideal light exposure scheme in which a tailored 3D pattern of light exposes an ink in a single shot.
- Light shone during 3D printing couples to the ink via electric-dipole-mediated light–matter interactions to dedicated trigger (photoinitiator) molecules; sometimes ordinary one-photon absorption suffices, yet often other processes such as multi-photon absorption or two-colour two-step absorption are needed to sufficiently localize the excitation in 3D space.
- Material formation from the ink following the light trigger is highly material dependent, with different chemical and physical processes involved for the formation of polymers, metals and semiconductors.
- Although researchers strive to improve the speed and resolution of 3D printing technologies, the formation of a certain voxel unavoidably requires delivering a certain light energy; therefore, increasing the number of voxels printed per unit time requires increasing light power.
- The challenges of 3D printing remain: enable ever finer feature sizes, increase print speed, open the door to more dissimilar materials and make 3D laser printers more compact and less expensive.

Introduction

The operation principle of 2D graphical ink-jet printers in many peoples' homes is quite simple: a liquid ink exits through a small hole in a nozzle and is ejected onto a piece of paper, in which it dries and forms a small picture element (pixel). To print many pixels per unit time, hundreds or thousands of nozzles are used in parallel and are mechanically moved with respect to the piece of paper as quickly as possible. In this manner, desktop printers operate at speeds of around 10^6–10^7 pixels s^{-1} with pixel sizes down to a few tens of micrometres. The operating principle of a 3D ink-jet material printer is similar, except that the 'ink' does not form a colour pixel in 2D but rather a material volume element (voxel) in 3D. Indeed, ink-jet-inspired printing[1–4] and related, more advanced mechanical approaches[5] have extensively been used for 3D material printing as well.

Given the existence of such straightforward mechanical means, why are there efforts to develop techniques that use light to act on a photosensitive ink for 3D printing? First, the quanta of light, photons, have no rest mass. It is, thus, possible to move a focus of light at speeds even greater than the speed of light[6], which would be impossible with a massive mechanical nozzle. Second, light together with an appropriately chosen light–matter interaction can be used as a trigger signal that locally starts a chemical reaction, forming a material at a particular spot. When this formation is completed, the light may well have triggered many other reactions at different spots already. Third, a bright spot of light can be positioned inside a material rather than just near its surface. Although irrelevant for 2D printing, this aspect is highly advantageous for 3D printing inside of transparent inks. Fourth, one can readily form many thousands or even millions of spots of light, which can be seen as a large assembly of 'local nozzles of light' in 3D. Fifth, the size of a light spot in the optical far-field is approximately half the wavelength of light, which can be as small as a few hundreds of nanometres for visible light. Adopting super-resolution tricks from optical microscopy[7–9] to optical printing[10–16], the wavelength of light is no longer a conceptual limitation. When combined, these five aspects give optical approaches quite an edge over mechanical methods.

However, simply pointing a laser beam into a suitable photosensitive ink is insufficient for 3D printing. The material would cure along the entire length of the laser beam instead of achieving a single confined voxel or a targeted 3D microstructure. Since the 1970s, many ideas emerged that ensure the wanted localization in space. In 1974, David E. H. Jones wrote in his column in *New Scientist* magazine: "Two different laser-beams traversing the tank would then form a solid spot of polymer at the point of their intersection. By scanning this point around, any type of solid object at all could be made up: even complex interlocking and re-entrant shapes quite impossible to mould."[17] In 1977, a closely related idea was patented[18]. However, neither of these works described in detail the physics of the nonlinear light–matter interaction that would lead to the anticipated solidification of a material exclusively at the spot in three dimensions in which the two laser beams with two different colours intersect. In 1993, 3D data storage using this idea was demonstrated[19]; two-colour 3D laser printing on the macroscale[20] was demonstrated in 2020 and on the microscale[21] in 2022.

In the meantime, a variety of other approaches to confine 3D-printed voxels emerged. In 1981, layer-by-layer fabrication was demonstrated, both point-by-point and by 2D images using a one-photon absorption process[22]. In 1984, 3D stereolithography[23] using one-photon absorption of a single colour of light from a continuous-wave source was patented. In stereolithography, the intensity of laser beam decays exponentially in the material, leading to a confined voxel. In 1997, 3D laser printing on the microscale and nanoscale using two-photon absorption of light induced by tightly focused intense femtosecond laser pulses was reported[24]. In 2000, intricate 3D periodic architectures were realized in a single nanosecond laser pulse by the tailored interference of four collimated laser beams and ordinary one-photon absorption[25]. Reverse tomographic projection was conceptualized in a 2016 patent application[26], a precursor to it was presented in 2017 (ref. 27) and complete versions were realized a few years later[28,29]. In these techniques, in the spirit of inverse tomography, a sequence of exposures with non-interfering 2D images from different directions is added up to approximate a targeted 3D object. Today, it has become hard for non-experts to see the similarities and differences in the physics of a plethora of light-based 3D printing approaches and to appreciate their conceptual pros and cons.

This Review aims at changing this situation. It provides an introduction into the principles of 3D printing with light, gives an overview on the state-of-the-art and points to future physics challenges and opportunities. We organize our discussion logically rather than historically into three steps: spatiotemporal modalities to expose matter by light, relevant light–matter interactions of photo-switches and mechanisms triggered by these photo-switches to locally form a targeted material in 3D. In other words, we discuss how complex patterns

of light can be created in three spatial dimensions and time, and then how the corresponding spatiotemporal distribution of photons can be translated into a material pattern, that is, into a 3D-printed object. In the jargon of 3D printing, the first step is the exposure by light, the second step leads to a deposited exposure-dose profile, and the third step translates this dose profile into a material.

Shaping spatiotemporal light patterns

Conceptually, a direct way to create any desired 3D light intensity pattern $I(\mathbf{r}, t)$ (with units W m^{-2}) is to use a Fourier transform, exploiting the superposition principle of light waves. Doing so requires superposing an infinite number of plane waves of light with different wavevectors $\mathbf{k}$ and complex-valued Fourier transform electric-field vectors $\tilde{\mathbf{E}}(\mathbf{k}, \omega)$ (Fig. 1) to arrive at the 3D intensity distribution $I(\mathbf{r}, t) \propto \langle \mathbf{E}(\mathbf{r}, t) \rangle^2$, where the total real-space (real-valued) electric field vector of light is $\mathbf{E}(\mathbf{r}, t)$, with real-space coordinate vector $\mathbf{r}$ and time t (Fig. 2). Here, $\langle ... \rangle$ refers to the average over one optical cycle. The Fourier transform leads to the integral

$$I(\mathbf{r}, t) \propto \langle \mathbf{E}(\mathbf{r}, t) \rangle^2 \propto \left| \int_{-\infty}^{\infty} \int_{-\infty}^{\infty} \int_{-\infty}^{\infty} \tilde{\mathbf{E}}(\mathbf{k}, \omega) \exp(\mathrm{i}(\mathbf{k} \cdot \mathbf{r} - \omega t)) \mathrm{d}k_x \mathrm{d}k_y \mathrm{d}k_z \right|^2 \quad (1)$$

where ω is the angular frequency of light, which is connected to $\mathbf{k} = (k_x, k_y, k_z)$ via the dispersion relation of light $\omega^2/\mathbf{k}^2 = c^2$, with the speed of light c in the ink in which light propagates. In what follows, we approximate $c = c_0/n$ to be real valued, equivalent to a real refractive index n, that is, we treat the inks as weakly absorbing.

We emphasize again that, along these lines, any arbitrary $I(\mathbf{r}, t)$ could be created. If a suitable ink is subjected to this exposure by light, one could 3D print any 3D object in a single-shot exposure. However, realizing the superposition in equation (1) is challenging experimentally. One would need a very large number of partial waves and, hence, directions of light. Furthermore, one would need to control the amplitude, polarization and phases of all the partial waves (as $\tilde{\mathbf{E}}(\mathbf{k}, \omega)$ is complex valued) (Fig. 1a). Many different moduli $|\mathbf{k}| = k$ correspond to a broad range of frequencies $\omega = ck$ of light, equivalent to complicated optical-pulse profiles in the time domain. In this ideal form, 3D printing has not been performed yet with light, though it has been approached acoustically[30]. However, all the methods we discuss below can be seen as attempts to come close to this ideal of using a single volumetric exposure by coherent light to arrive at an arbitrary non-periodic or periodic 3D-printed object[31,32].

Interference lithography

Perhaps the closest attempt is 3D interference lithography (or holographic lithography). Here, we restrict ourselves to monochromatic light at angular frequency $\omega = \omega_0$ and to merely four ($m = 0,1,2,3$) plane waves or laser beams with wave vectors $\mathbf{k}_m$ and $|\mathbf{k}_m| = \omega_0/c$ (Fig. 1b). This simplification leads to the time-independent (because $|\exp(\mathrm{i}\omega t)|^2 = 1$ in equation (1)) intensity profile

$$I(\mathbf{r}) \propto \left| \sum_{m=0}^{3} \tilde{\mathbf{E}}_m \exp(\mathrm{i}\mathbf{k}_m \cdot \mathbf{r}) \right|^2 = \sum_{m,n=0}^{3} A_{mn} \exp(\mathrm{i}\mathbf{G}_{mn} \cdot \mathbf{r}), \quad (2)$$

where $\mathbf{G}_{mn}$ are the reciprocal lattice vectors (formed from beams m and n). One of the four wave vectors, say, $\mathbf{k}_0$, serves as a reference. The other three wave vectors can be chosen such that the three vectors $\mathbf{G}_{10} = \mathbf{k}_1 - \mathbf{k}_0$, $\mathbf{G}_{20} = \mathbf{k}_2 - \mathbf{k}_0$ and $\mathbf{G}_{30} = \mathbf{k}_3 - \mathbf{k}_0$ span any of the 14 periodic Bravais lattices in 3D[33]. The terms with $m = n$ in equation (2) lead to a spatially constant intensity background. The form factors $A_{mn} = \tilde{\mathbf{E}}_m \tilde{\mathbf{E}}_n^* = A_{nm}^*$ determine the shape of the interior of one unit cell. They describe that for each of the four laser beams, one can additionally choose its intensity and its polarization of light, leading to 12 scalar parameters. If one aims to print a specific crystal lattice, one needs to solve a difficult inverse problem, namely to identify the combination of 12 parameters that leads to a desired lattice or that at least come close to it. For example, this problem has been solved in the context of complete photonic-band gap crystals in 3D[34]. For periodic metamaterials[35], this theoretical problem has generally not been solved to date, but the approach has been used experimentally[36,37]. Note that the wave vectors $\mathbf{k}_m$ in equation (2) refer to the inside of the ink with refractive index n rather than to air. Therefore, specially shaped interfaces to air are generally necessary to avoid limitations owing to the critical angle of total internal reflection[38–40].

One issue of the four-beam approach is that the period of the lattice is approximately half the wavelength of light $\lambda = 2\pi/k$. For visible light, this period is in the range of only a few hundred nanometres. However, for mechanical metamaterials[35,41], for example, periods of some tens of micrometres may be wanted. A solution is a triple-exposure scheme, by which any period larger than π/k can be achieved. This sequential (hence, incoherent) exposure leads to the sum $I(\mathbf{r}) = \sum_{i=1}^{3} I_i(\mathbf{r})$. It has been shown that this sum also allows for printing any 3D Bravais lattice[42], with reduced flexibility in tailoring the shape of the unit cell, but increased flexibility in choosing the lattice period. Extensions of holographic lithography towards non-periodic architectures[43–45] and more beams[31] have been explored (Fig. 2a).

Spatial focusing

The opposite of volumetric interference of light is to use equation (1) to obtain only a single tight focus of light via a lens (Fig. 1c), leading to a single 3D-printed voxel (Fig. 2b). For (quasi-)monochromatic light with $|\mathbf{k}| = k = \omega/c = \omega_0/c = \text{const.}$, in spherical coordinates with polar angle ϑ and azimuthal angle φ, and for using a single lens ($\vartheta \in [0,\pi]$), we have the time-independent intensity pattern[46]

$$I(\mathbf{r}) \propto \left| \int_0^{\arcsin\left(\frac{\mathrm{NA}}{n}\right)} \int_0^{2\pi} \tilde{\mathbf{E}}(k, \vartheta, \varphi) \exp(\mathrm{i}\mathbf{k} \cdot \mathbf{r}) \mathrm{d}\varphi \mathrm{d}\vartheta \right|^2, \quad (3)$$

with $k_x = k \sin\vartheta \cos\varphi$, $k_y = k \sin\vartheta \sin\varphi$, $k_z = k \cos\vartheta$ and $x = r \sin\vartheta' \cos\varphi'$, $y = r \sin\vartheta' \sin\varphi'$ and $z = r \cos\vartheta'$, with $r = |\mathbf{r}|$. If one uses a single ideal optical lens with numerical aperture NA = n and constant phase and modulus of $\tilde{\mathbf{E}}(k, \vartheta, \varphi)$, the lateral full width of the intensity profile $I(\mathbf{r}, t)$ is on the order of half the wavelength, $\lambda/2 = \pi/k$ (ref. 47). The axial full width is twice as large because only half of the solid angle of all wavevectors of light $\mathbf{k}$ is used, leading to a focus aspect ratio of 2 (ref. 48). In reality, the focus aspect ratio for a single lens is typically approximately 2.5 when using high-quality immersion microscope objective lenses with NA ≈ 1.4 and $n \approx 1.5$ (ref. 49). If the refractive index of the ink is not matched to the microscope lens, the aspect ratio quickly deteriorates, owing to abberations[50,51]. This behaviour is undesirable because it introduces a pronounced anisotropy from the start. Conceptually, aberrations preventing the ideal focus can be pre-compensated using tailored phase profiles of the incident light (as discussed below).

Complex 3D objects can be printed by exposing the ink not only to a single focus centred at position $\mathbf{r}_1$ but also sequentially (hence,

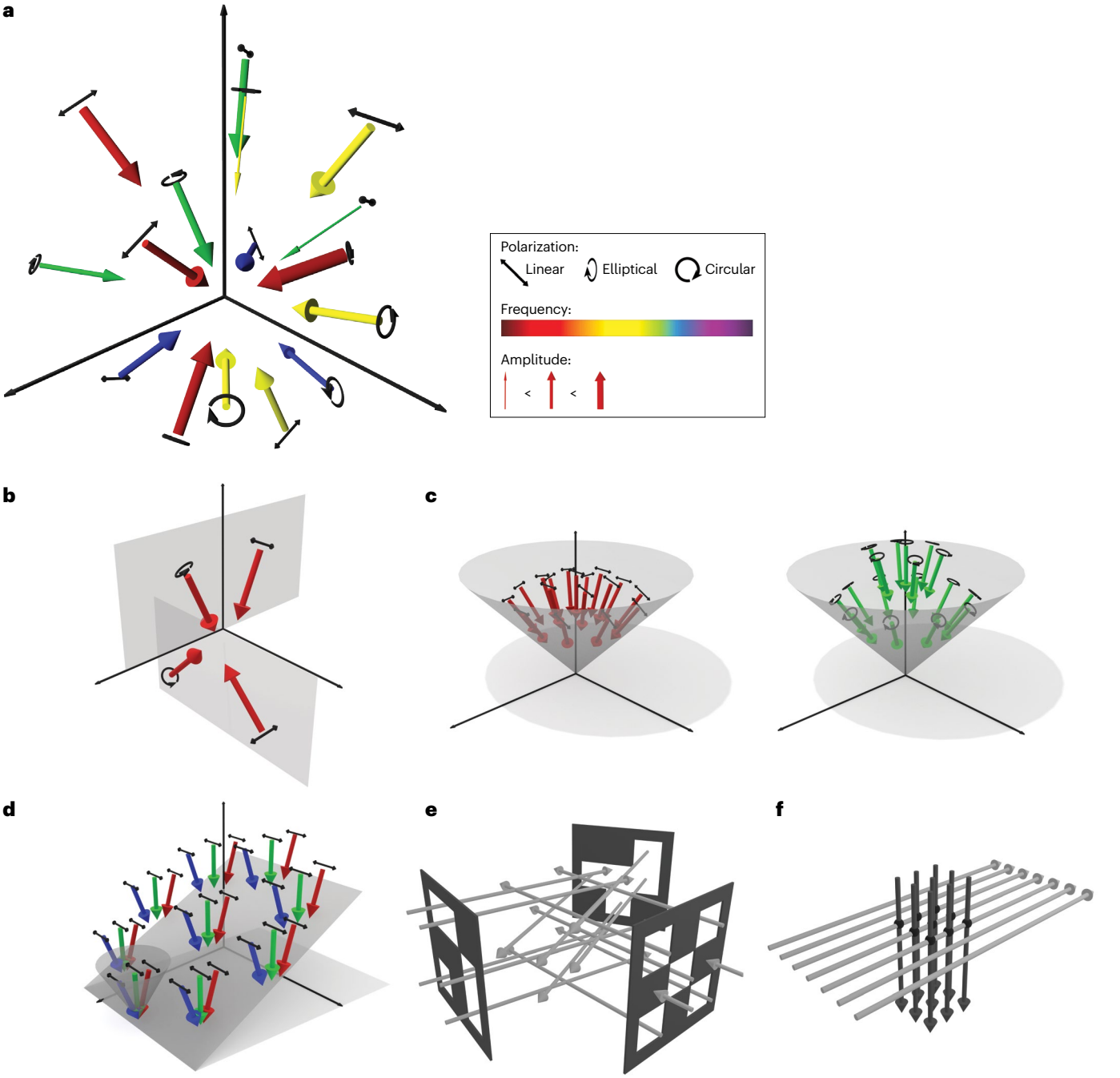

incoherently) to many different foci of light with centre positions $\mathbf{r}1, \mathbf{r}_2 ..., \mathbf{r}_N$. In doing so, one must appreciate though that the laser focus according to equation (3) has long spatial tails, making it necessary to use nonlinear forms of light–matter interaction to avoid massive accumulation effects (see 'Relevant light–matter interactions' section). For print processes near the surface of a bed of material[52,53], the long spatial tails are irrelevant.

A single ellipsoidal focus can be turned into more complex intensity patterns by introducing a phase mask into the conjugated plane of the lens that creates a non-constant distribution of the complex-valued Fourier coefficients $\tilde{\mathbf{E}}(k, \vartheta, \varphi)$ within the entrance pupil of the focusing lens. For example, $N \times N$ arrays of laser foci can be achieved[54–61] for faster printing. As another example, using relatively simple optical phase masks[62] (Fig. 1c) to create the corresponding $\tilde{\mathbf{E}}(k, \vartheta, \varphi)$, one can obtain 'inverted foci', in which the light intensity is zero at the position of the maximum of an ordinary focus (Fig. 2b). This zero-intensity point arises from destructive interference of two contributions phase-delayed by π and can be surrounded by intensity maxima in 3D. Such 'bottle-beam focus'[63] is crucial for 3D laser printing beyond the diffraction limit (see 'Relevant light–matter interactions' section). Many further differently shaped focus iso-intensity surfaces (Fig. 2b) can be obtained by adjusting $\tilde{\mathbf{E}}(k, \vartheta, \varphi)$ (refs. 64,65). For targeted

Fig. 1 | Partial wave representations of generating spatiotemporal light patterns for use in 3D printing. a, General case: illustration in **k**-space of the many possible partial waves that lead to the formation of an arbitrary 3D light pattern. Each partial wave indicates direction and phase (direction of arrow and distance from plot origin), as well as polarization, frequency and amplitude, all of which contribute to the resulting light field intensity, $I(\mathbf{r}, t)$. **b**, Interference lithography: partial wave representation of four-beam interference lithography in a two-plane geometry using linear and circularly polarized coherent beams as an example. Three-dimensional $I(\mathbf{r}, t)$ patterns are generated by interference of the beams. Three-dimensional interference lithography can be achieved with beams. **c**, Spatial focusing: the partial waves for spatial focusing are bounded by a cone representing the restriction of the finite numerical aperture of the focusing optics on the possible light directions. The spatial focusing of a linearly polarized Gaussian beam (left) and a circularly polarized 'bottle beam' (right) achieved by an annular π phase shift of the focusing waves are depicted. **d**, Spatiotemporal focusing: partial wave representation of spatiotemporal focusing for a linearly polarized beam at a single instance of time. Separated frequencies of a broad spectrum of light recombine together only at the spatial focus. The tilted plane is a guide to the eye outlining the spatial variance of the phase of the partial waves in the beam resulting from the diffraction grating typically used to separate the frequencies. Spatiotemporal focusing has a similar cone of focusing (though with reduced numerical aperture) as spatial focusing. **e**, Tomographic volumetric additive manufacturing: light ray representation of tomographic volumetric additive manufacturing depicting only three (of typically many) exposure angles by a projection of varying 2D light patterns. A 3D $I(\mathbf{r}, t)$ is created by the sum of the light intensities of the projected light rays. **f**, Layer-by-layer approaches: light ray representation of layer-by-layer printing in a light sheet configuration. Rays forming the print pattern (dark grey) intersect with different wavelength light sheet rays (light grey), creating a plane containing the target $I(\mathbf{r}, t)$ light pattern in 2D.

intensity profiles $I(\mathbf{r})$, inversion procedures such as the Gerchberg–Saxton algorithm[66,67] allow for iteratively computing $\tilde{\mathbf{E}}(k, \vartheta, \varphi)$. In this limited manner, one approaches complete volumetric 3D printing as suggested by equation (1), albeit combined with a number of sequential (hence, incoherent) point-like exposures with light[67–70].

Spatiotemporal focusing

A further step back into the direction of volumetric 3D printing according to equation (1) is to make use of incident optical pulses instead of continuous-wave light impinging onto a single lens, leading to the time-dependent intensity pattern

$$I(\mathbf{r}, t) \propto \left| \int_{k_{\min}}^{k_{\max}} \int_{0}^{\arcsin\left(\frac{\mathrm{NA}}{n}\right)} \int_{0}^{2\pi} \tilde{\mathbf{E}}(k, \vartheta, \varphi) \exp\left(\mathrm{i}\left(\mathbf{k}\cdot\mathbf{r} - \frac{k}{c}t\right)\right) \mathrm{d}\varphi \, \mathrm{d}\vartheta \, \mathrm{d}k \right|^2, \quad (4)$$

which is a generalization of equation 3. In the Fourier domain, an optical pulse corresponds to a distribution of angular frequencies ω (rather than to a fixed constant single frequency $\omega = \omega_0$ for monochromatic light).

Finding $\tilde{\mathbf{E}}(k, \vartheta, \varphi)$ for a desired pattern $I(\mathbf{r}, t)$ is not trivial[71]. It is, thus, perhaps best to consider an example[72,73]. Placing a diffraction grating at a conjugate focal plane of the focusing lens has two consequences. First, the different frequency components (or wavelength components) of an optical pulse are laterally spread across the conjugated plane of a lens, and all frequency components will again come together in the focal plane according to Fermat's principle (Fig. 1d). As a result, the optical pulse is stretched out in time outside of the focal plane and recovers its original duration only in the focal plane. Combined with nonlinear absorption of light (see 'Relevant light–matter interactions' section), the light–matter interaction can, thereby, be better confined to the focal plane[74]. Second, the grating tilts the laser-beam pulse front with respect to the focal plane. Hence, the pulse is reconstructed along a line which moves with velocity v perpendicular to the line within the focal plane[72] (Fig. 2c). As a result, different parts of the ink are sequentially exposed by light — as discussed above. The focus velocity $v = c(M \sin\alpha)^{-1}$, with the grating illumination angle α and the magnification of the imaging optics M, approaches and can even exceed the speed of light c (ref. 72). Importantly, the rapid motion of the line within the focal plane is not induced by mechanical motion of any component in the 3D printer.

So far, in addition to a grating[75], only spatial amplitude-only modulators have been used to influence $\tilde{\mathbf{E}}(k, \vartheta, \varphi)$ (refs. 74,76–78). In this case, to 3D print objects that are extended perpendicular to the focal plane, scanning and multiple sequential (incoherent) exposures by light are necessary (not to be confused with layer-by-layer printing discussed in the next section). When using spatial amplitude-and-phase modulators[79], entire 3D microstructures could be printed in a single exposure. Of course, in either case, their lateral extent (without moving the sample) is fundamentally limited by the finite field-of-view of the microscope objective lens.

Tomographic volumetric additive manufacturing (computed axial lithography)

The intensity pattern $I(\mathbf{r}, t)$ in equation (1) for fully volumetric 3D printing arises from the interference of a large number of partial waves of light that irradiate an ink. Likewise, equations (2) and (4) and some forms of equation (3) require the interference of light. Is it conceptually possible to achieve volumetric 3D printing with light without interference, that is, with incoherent light?

For illustration, one can view a collimated beam of light as a collection of rays of light propagating in the same direction. Two-dimensional spatial information (image) can be encoded by providing a grayscale value to each ray of light. Let the intensity $I_1(\mathbf{r})$ corresponding to image 1 be constant and non-zero only along a straight line, and the intensities $I_m(\mathbf{r})$ refer to $m = 1, 2, \ldots, N \gg 1$ 2D images. The direction of the light rays for each image are different and we assume that there is no coherence between the light corresponding to different images. Suppose that all these light rays are switched on at the same time. They incoherently add up and the time-independent total intensity pattern is

$$I(\mathbf{r}) = \sum_{m=1}^{N} I_m(\mathbf{r}) = \sum_{m_{\mathrm{image}}=1}^{N_{\mathrm{image}}} \sum_{p_{\mathrm{pixel}}=1}^{N_{\mathrm{pixel}}} I_{m_{\mathrm{image}}, p_{\mathrm{pixel}}}(\mathbf{r}). \quad (5)$$

Can one construct any arbitrary targeted complex 3D pattern $I(\mathbf{r})$ along these lines? Based on the tomographic reconstruction principle[80], the answer is yes — at least approximately. As illustrated in Fig. 1e, the N rays can arise from N_{image} different 2D images, each with N_{pixel} pixels, that are projected into a tank of ink from N_{image} different directions that lie within a single plane, leading to a total number of $N = N_{\mathrm{image}} N_{\mathrm{pixel}}$ light rays in equation (5). The intensity patterns of the 2D images involved can be calculated by using a solution of the inverse problem to the Radon transformation[81–83]. An approximation lies in

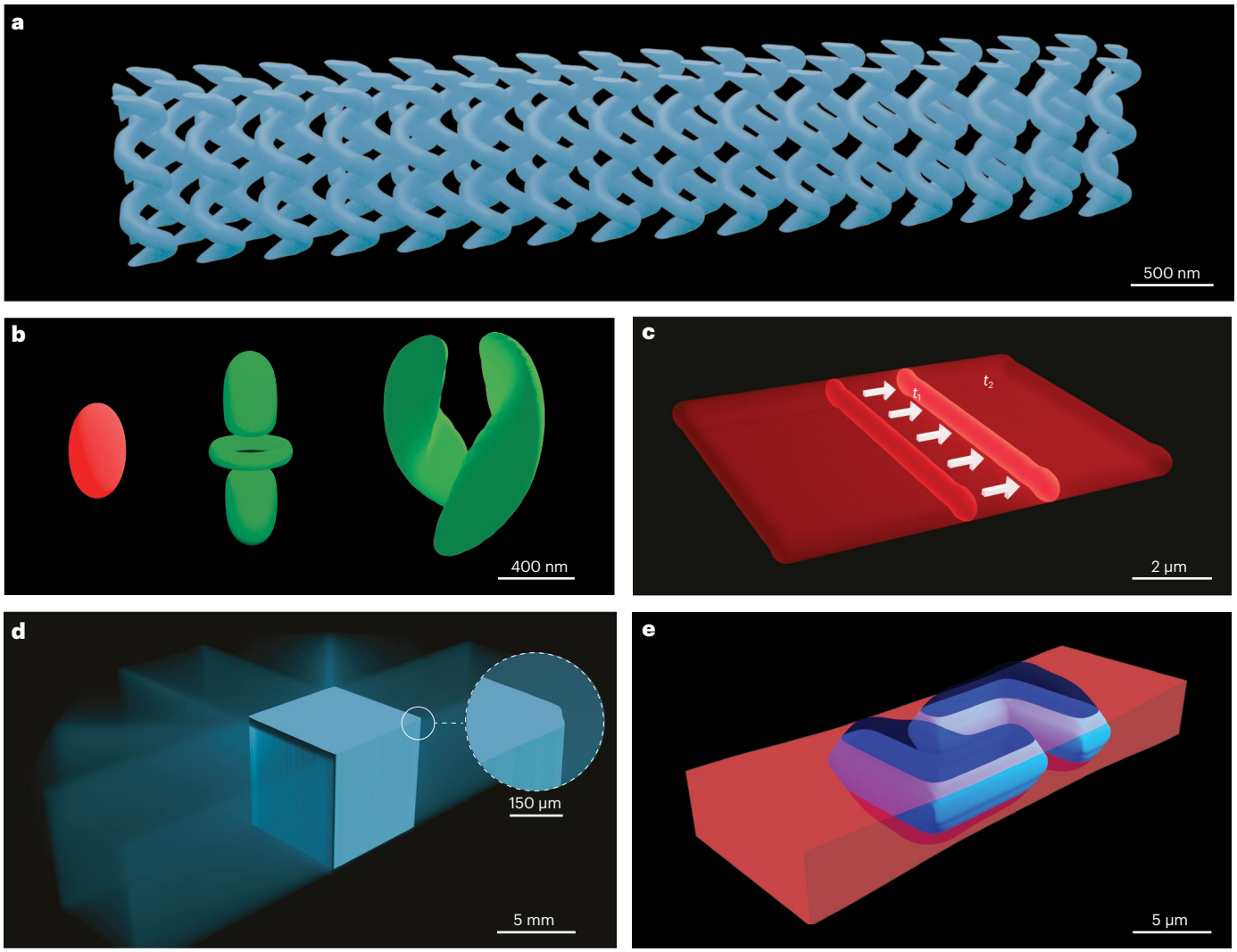

Fig. 2 | Iso-intensity surfaces of light patterns generated via various light shaping processes. a, Interference lithography: iso-intensity surface of six (linearly polarized) beams and one (circularly polarized) beam interfering with each other to generate a helical-shaped light structure[31]. **b**, Spatial focusing: iso-intensity surface of spatially focused Gaussian beam typically used for scanning-based printing (left), 'bottle beam' iso-intensity generated using an annular π phase shift of the beam typically used for inhibition of printing (centre), and double helix iso-intensity formed by spatially designed beam intensity and phase profile demonstrating the possibilities enabled by spatially engineering the beam properties (right)[32]. **c**, Spatiotemporal focusing: iso-intensity layer of a single spatiotemporally focused rectangular pattern. At any one instant, only a single 'line'-like iso-intensity exists, which scans (from t_1 to t_2) across the focal plane to form the pattern. **d**, Tomographic volumetric additive manufacturing: iso-intensity of the sum of many (only five shown) 2D projected light patterns from different angles for tomographic volumetric additive manufacturing. Inset shows artifacts when constructing sharp features using incoherent light. **e**, Layer-by-layer approaches: intersecting iso-intensities for layer-by-layer printing using a light sheet. The printed volume exists in which the light sheet (red iso-intensity) and the perpendicularly projected pattern (blue iso-intensity) intersect.

that 'unphysical' negative intensities, $I_m < 0$, generally arise from this algorithm, which are then set to zero. This step leads to deviations between the targeted and the printed structure. In this conceptual form, the approach would be fully volumetric in that the 3D light pattern is created in a single shot (Fig. 2d). In practice, one instead uses N_{image} sequential exposures by light[28,29]. In this case, the optical setup projecting an image is fixed and a cylindrical tank containing the ink is rotated around its centre axis. The resulting total exposure of the ink does depend on the type of light–matter interaction[84] which we discuss in 'Relevant light–matter interactions' section.

Layer-by-layer approaches

Finally, 3D printing can also be achieved by projecting a conventional 2D optical image into a thin layer[85,86] (Fig. 1f). The thickness of this layer can, for example, be controlled by the optical absorption length in the ink. After mechanical delamination of this layer from the underlying substrate[87,88], the next 2D layer is printed. The stack of 2D layers eventually forms the 3D object. The delamination time limits the printing speed in commercially widespread stereolithography[18,22,23]. This limitation is overcome in continuous liquid-interphase printing[89], in which the printed layer does not adhere to the underlying substrate[90–92].

Light-sheet 3D laser printing[20,21] is related, but the 2D optical image with intensity pattern $I_1(\mathbf{r})$ at wavelength λ_1 is not projected onto a surface but rather inside the volume of the ink into the plane of a thin light-sheet with intensity $I_2(\mathbf{r})$ at wavelength λ_2 that is formed by a cylindrical lens (Fig. 2e). By virtue of an optical nonlinearity of the ink (see 'Relevant light–matter interactions' section), the excitation can be approximately $\propto I_1(\mathbf{r})I_2(\mathbf{r})$. Therefore, the light-sheet $I_2(\mathbf{r})$ 'gates' the excitation and only a thin 2D layer is effectively exposed by light. By scanning the z-position of this layer with respect to the ink, 3D objects can be printed. Compared with stereolithography, no delamination is required. Furthermore, because the object is printed inside the volume of the ink, objects exceeding the projection area can be stitched in sequential prints.

For all these layer-by-layer 3D printing approaches, the wave nature of light is not necessary conceptually but does clearly limit the achievable spatial resolution via diffraction.

Relevant light–matter interactions

During the 3D printing process, the light field inside of the liquid and transparent ink couples to certain molecules. In most cases, these molecules are 'initiators' intentionally added to the ink. In fewer cases, the liquid (monomer) itself couples to the light[93–96]. The coupling can be described via the usual electric-dipole interaction term[97,98] in the system's Hamiltonian

$$\hat{H} = \hat{H}_{\text{ink}} - \sum_{i,f} \mathbf{d}_{if} \cdot \mathbf{E}(\mathbf{r}, t). \tag{6}$$

The integer indices i and f run over the relevant initial and final electronic states of the ensemble of (initiator) molecules with corresponding vectorial electric-dipole moment(s) $\mathbf{d}_{if}$. This interaction is generally followed by relaxation processes within the initiator, leading to the population of a relevant excited state of the system, which triggers chemical reaction(s) leading to a printed material (described in 'Mechanisms of material formation' section). We define the dimensionless instantaneous local light-exposure dose $D(\mathbf{r}, t) \in [0,1]$ at time t as the quantum mechanical probability with which this relevant state is populated. $D(\mathbf{r}, t_{\text{exp}})$ is the local dose after completing the light-exposure process at time t_{exp}.

According to equation (6), the initiators only 'see' the electric field of the light and not directly its magnetic field. Hence, the relevant intensity of light is the optical-cycle-averaged squared electric field $I(\mathbf{r}, t) \propto \langle \mathbf{E}(\mathbf{r}, t) \rangle^2$ rather than the intensity in the sense of the cycle-averaged Poynting vector of light, $I'(\mathbf{r}, t) = \langle \mathbf{E}(\mathbf{r}, t) \times \mathbf{H}(\mathbf{r}, t) \rangle$ (ref. 99). The latter contains the electric-field and the magnetic-field vector $\mathbf{H}(\mathbf{r}, t)$ of light. Whereas the two quantities are equal for a single plane wave of light, they are quantitatively and qualitatively different in general. For example, for a diffraction-limited spatial or spatiotemporal focus of light (see the previous section), the symmetry and the qualitative shape of the focal region is distinctly different, thereby directly influencing the 3D printing process. Therefore, we have consistently considered $I(\mathbf{r}, t) \propto \langle \mathbf{E}(\mathbf{r}, t) \rangle^2$ in the previous section. This reasoning tacitly assumes that the orientations of the initiator molecule's electric-dipole vectors $\mathbf{d}_{if}$ in the ink are random. This assumption is typically fulfilled. If not, one would have to work with $\mathbf{E}(\mathbf{r}, t)$ instead of $I(\mathbf{r}, t)$.

For initiator molecules with many energy levels and many radiative and non-radiative transitions between them (Fig. 3), getting from $I(\mathbf{r}, t)$ to $D(\mathbf{r}, t)$ is generally not trivial. Density-functional theory has lately been catching up on treating such systems microscopically[100], but a bulk of work over the years has rather used simplified semi-phenomenological rate-equation descriptions for the kinetics[101,102], partly combined with diffusion equations to describe transport processes[103,104].

What dependence between I and D is required depends on the printing modality. For example, for interference lithography, simple local linear absorption of light suffices according to

$$D(\mathbf{r}) \propto I(\mathbf{r}). \tag{7}$$

This is not true for scanning 3D laser printing. There, such light–matter interaction leads to excessive accumulation of excitation in the long-reaching tails of the laser focus, making 3D printing generally impossible[105]. A dependence

$$D(\mathbf{r}) \propto I^2(\mathbf{r}) \tag{8}$$

strongly reduces the influence of these tails and enables 3D printing[106]. Such a dependence can be obtained in many ways. Originally,

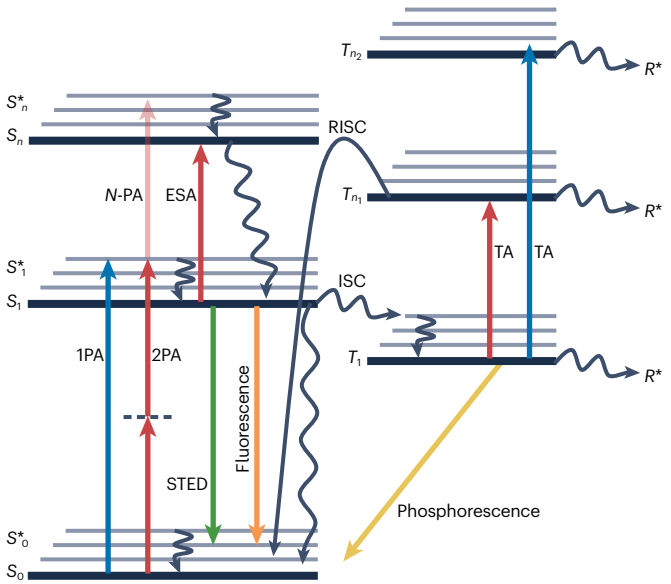

Fig. 3 | Energy level diagram of light-matter interactions for 3D printing. Light-based 3D printing requires a light-sensitive material (typically a photoresin containing a 'photoinitiator' molecule) that elicits a material response (typically leading to a polymerization reaction) after light exposure. The potential responses of the photoinitiator are complex. First, the molecule absorbs the light via one-photon (1PA) or two-photon (2PA) absorption from the ground state (S_0) to a vibrationally excited state (S_1^*) followed by a fast vibrational relaxation to the first excited state (S_1). Most commonly, the molecule will then either emit fluorescence and return to the ground state or undergo intersystem crossing (ISC) to the triplet manifold. From the lowest triplet state (T_1), it is usually assumed to either relax non-radiatively to the ground state, emit phosphorescence and return to the ground state, or generate a radical molecule (R^*) that initiates the print process. Alternatively, the molecule can absorb more light from the T_1 state via triplet state absorption (TA), raising it to a higher triplet state (T_{n_1}), which could either generate a radical or undergo reverse intersystem crossing (RISC) back to the singlet manifold, or an even higher triplet state (T_{n_2}), which can do the same. There are also possibilities for the molecule to absorb $N > 2$ photons (N-PA) from the ground state or absorb light from the excited singlet state (ESA) to an even higher singlet state (S_n). A second light source can also induce stimulated emission depletion (STED) from the S_1 state. STED-inspired printing utilizes those optically active molecular pathways that avoid generating radicals such as STED and TA followed by RISC.

two-photon absorption[107] was considered for 3D printing[108]. In this process, the light field (while switched on) induces a 'virtual' or dressed state between the ground state and an excited state of the initiator molecule. Two-photon absorption can be seen as the simultaneous absorption of two photons. N-photon absorption is proportional to the imaginary part of the $(2N-1)$th order nonlinear optical susceptibility[109]. To make two-photon absorption sufficiently efficient for 3D printing, intensities of light in the range of $I = 10^{12}$ W cm^{-2} = 1 TW cm^{-2} are routinely achieved in 3D printers, by tightly focused femtosecond laser pulses.

Much work has gone into identifying initiator molecules with large two-photon absorption coefficients, both experimentally and theoretically[110–115], and yet more importantly, into obtaining large ratios of $D(\mathbf{r})/I^2(\mathbf{r})$ (which is a related but not equivalent parameter)[105]. However, complex processes in the initiator molecule can also lead to $D(\mathbf{r})/I^N(\mathbf{r})$ with exponent $N > 2$ and even $N > 3$ for two-photon absorption followed by excited-state one-photon absorption and non-radiative relaxation processes[102,116,117]. Such behaviour is beneficial because it further reduces the influence of the long-reaching tails of the laser focus.

More recently, much attention has been devoted to obtaining $D(\mathbf{r}) \propto I^2(\mathbf{r})$ by means other than two-photon absorption, and especially to obtaining such behaviour with low-power continuous-wave lasers rather than with bulky and expensive femtosecond lasers. One way to achieve this is by controlling the ink chemistry and diffusion[93,118–120]. Another is to replace the virtual intermediate state in two-photon absorption by a 'real' electronic state, the lifetime of which can be many orders of magnitude larger (from microseconds to seconds) than typical femtosecond pulse durations. In this approach, the two absorbed photons need not be absorbed simultaneously (more precisely, within the pulse duration) but can rather be absorbed sequentially in two consecutive one-photon absorption steps, hence the name 'two-step absorption'[21,101]. Along these lines, high-quality 3D printing with diffraction-limited spatial resolution has been obtained experimentally using continuous-wave semiconductor laser diodes with powers in the range of merely 100 μW (ref. 101). Another example for using two-step absorption is light-sheet 3D printing[21], which uses closely related two-step processes, albeit with a different energetic position of the intermediate state, which can lead to an exposure dose depending on two different continuous-wave light intensity distributions at two different laser frequencies, in the simplest form according to

$$D(\mathbf{r}) \propto I_1(\mathbf{r}) I_2(\mathbf{r}). \tag{9}$$

Today, a variety of one-colour and two-colour two-step-absorption initiator molecules and inks based thereupon is available[121], but the search for yet better molecules is ongoing. Alternative mechanisms to obtain nonlinear behaviours of the type $D(\mathbf{r}) \propto I^2(\mathbf{r})$ are up-conversion luminescence followed by one-photon absorption[122–127] and triplet–triplet annihilation[128,129] (see the review in ref. 130).

Although tomographic volumetric additive manufacturing approximately works for simple one-photon absorption of light according to $D(\mathbf{r}) \propto I(\mathbf{r})$, it would benefit from a dependence according to $D(\mathbf{r}) \propto I^2(\mathbf{r})$ so that unwanted dose accumulation from many exposures with small $I(\mathbf{r})$ are reduced. Technically, negative dose contributions arising from the Radon transformation could be reduced, thereby bringing the actually printed object closer to the targeted one. Likewise, a dependence $D(\mathbf{r}) \propto I^2(\mathbf{r})$ would also suppress the influence of the constant intensity background in interference lithography.

Why stop at $D(\mathbf{r}) \propto I^2(\mathbf{r})$ and not consider $D(\mathbf{r}) \propto I^N(\mathbf{r})$ with $N \gg 2$? Such a larger exponent would further suppress the accumulation of exposures with small intensities of light. N-photon absorption with N as large as 6 has been achieved[116]. However, it has so far been difficult to achieve a comparable ease of operation and width of the process window. At some point, so much heat is deposited that the ink locally evaporates, leading to a micro-explosion[116,131]. We note in passing that although pronounced local heating ($I(\mathbf{r}, t) \rightarrow T(\mathbf{r}, t) \rightarrow$ material with temperature T) is undesirable for many 3D printing modalities, it has lately been used as the key mechanism for new 3D printing modalities instead of $I(\mathbf{r}, t) \rightarrow D(\mathbf{r}, t) \rightarrow$ material (as discussed below).

Above, we have only considered processes in which the local exposure dose D increases owing to excitation by light. In many situations, it is also desirable to reduce the local dose by some means of de-excitation. These situations include reduction of dose accumulation owing to long-reaching focus tails in spatial and spatiotemporal focusing, as well as in tomographic volumetric additive manufacturing. In optical microscopy[132], de-excitation processes such as stimulated-emission depletion (STED) have been revolutionary in that they make it possible to systematically break the Abbe diffraction barrier of spatial resolution at a given non-zero wavelength of light[8]. The STED idea can directly be carried over from optical microscopy to optical 3D printing[11,133,134] (see also reviews in refs. 14,15,49).

In our nomenclature, using excitation with a first intensity pattern $I_1(\mathbf{r})$ at one frequency of light $\omega = \omega_1$ and de-excitation with a differently shaped intensity pattern $I_2(\mathbf{r})$ at $\omega = \omega_2$, the exposure dose D could, for example, follow the simple form[49]

$$D(\mathbf{r}) \propto \frac{I_1^N(\mathbf{r})}{1 + \frac{I_2(\mathbf{r})}{I_{\mathrm{ref}}}}, \tag{10}$$

where I_{ref} is the reference intensity for I_2, at which the mathematical fraction (10) has decreased to half of its value for $I_2 = I_{\mathrm{ref}}$ as compared to when $I_2 = 0$. I_1 could be a focus of light with its intensity maximum at around $\mathbf{r} = 0$ (Fig. 2b), whereas I_2 could be a bottle-beam focus (Fig. 2b) with zero intensity at this point, but non-zero intensity in the 3D periphery of this point. STED in the strict sense of using depletion by stimulated emission of light has been realized in 3D printing[134,135] and has contributed to resolution improvement, but de-excitation processes other than STED tend to be yet more important in 3D printing with light[12,16,102].

Above, we have already seen for one-colour and two-colour two-step absorption that excited-state absorption can be very pronounced as the transition probability $\propto \mathbf{d}_{if}^2$ (see equation (6)) for such optical transitions can be two orders of magnitude larger than those of the transitions from the ground state of the initiator molecule[136]. However, from an excited state, the electron can not only relax non-radiatively towards a relevant excited state, the population of which we have called the exposure dose D, but it can also relax non-radiatively to other states, including relaxation eventually back to the ground state of the molecule. In the language of chemistry, such process is referred to as reverse intersystem crossing from the triplet manifold back to the singlet manifold.

Although the above description

$$I(\mathbf{r}, t) \rightarrow D(\mathbf{r}, t) \tag{11}$$

in terms of an exposure dose D as the quantum mechanical population probability of a relevant electronic state is suitable for many situations in modern 3D printing with light, especially for printing organic polymers, it is not applicable for all. Lately, processes have

been described in which rather the local rise of the temperature T in the ink according to

$$I(\mathbf{r}, t) \rightarrow T(\mathbf{r}, t) \tag{12}$$

starts a chemical reaction in the ink that leads to the formation of polycrystalline or crystalline inorganic material[137]. For the formation of metals, both processes (11) and (12) matter[138]. In process (12), the temperature profile follows the usual diffusion equation of heat, into which the local light intensity $I(\mathbf{r}, t)$ enters as a source term. Usually, this source term can be assumed as being $\propto \alpha_1(\mathbf{r}, t)\, I(\mathbf{r}, t)$, with the local one-photon absorption coefficient $\alpha_1(\mathbf{r}, t)$, which may, however, explicitly depend on time during the ongoing printing process. This dependence means that light–matter interaction itself is quite simple in these cases, but the processes triggered thereby can become very complex – an aspect into which we dive in the following section.

Mechanisms of material formation

The processes leading from the exposure dose $D(\mathbf{r}, t)$ and/or from the temperature profile $T(\mathbf{r}, t)$(both arising from the light-intensity profile $I(\mathbf{r}, t)$ described previously) to the local formation of material are generally complex. They are also rather different for different types of materials (polymers, metals and semiconductors) and bring us into the realm of the chemistry and materials science of 3D printing with light. Several reviews focusing on these aspects have been published[139–142]. Hence, here we only briefly touch upon them. The processes below can also be combined to arrive at multi-material microstructures and nanostructures[143–145], as reviewed in ref. 146.

We start with polymers (Fig. 4a–e) for which a simple yet useful phenomenological description is the so-called threshold model. Mathematically, it states that a certain critical threshold dose $D_{th} \in [0,1]$ exists. If the local dose $D(\mathbf{r}, t_{exp})$ at a point in time $t = t_{exp}$ after completing the

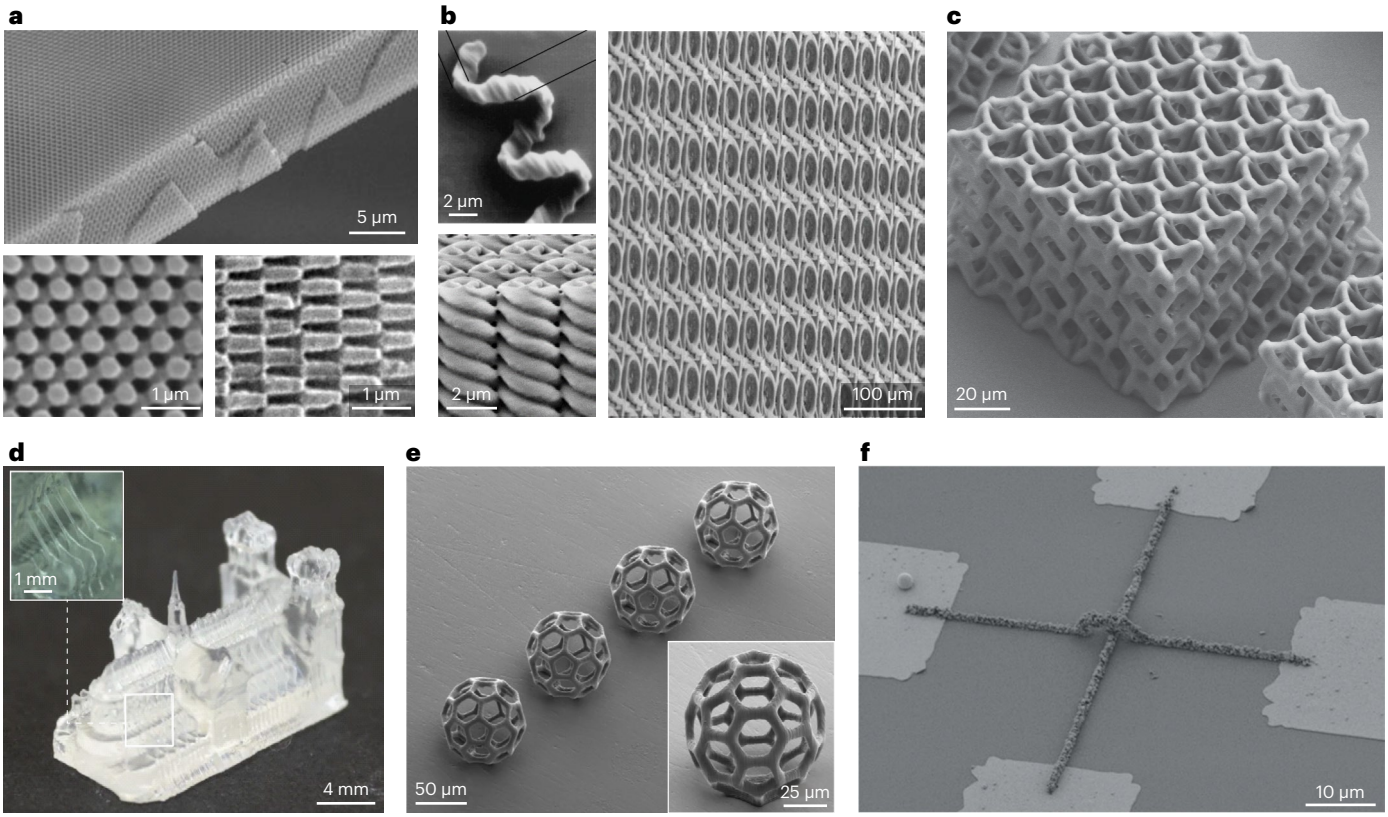

Fig. 4 | Three-dimensional-printed structures using light-based printing processes. a, Interference lithography: photonic crystal lattice printed using a four-beam interference lithography process in 10 µm thick photoresist (upper panel). Top surface of photonic crystal ((111) crystal plane) (lower left) and side image of photonic crystal ((111) cleavage plane) (lower right). **b**, Spatial focusing: 3D helix printed using two-photon absorption by scanning a laser focus inside a photoresist (upper left). A 3D chiral metamaterial composed of about 3×10^{11} voxels fabricated by scanning an array of 3×3 Gaussian laser foci inside a photoresin (right). Hollow cast of a triple helix shape fabricated inside a photoresin using stimulated-emission depletion-inspired lithography (Gaussian printing laser focus overlapped with a 'bottle-beam' depletion laser focus) to improve printing resolution (lower left). **c**, Spatiotemporal focusing: 3D lattice structure of $5 \times 5 \times 3$ unit cells fabricated using a continuous translation while projecting spatiotemporally focused 2D light patterns for multi-photon absorption in a photoresin. **d**, Tomographic volumetric additive manufacturing: model of Notre Dame cathedral fabricated by projecting 2D images into a rotating container of photoresin. The images are calculated to provide angularly dependent individual 3D light exposures that combine to form the 3D shape. Inset: increased magnification of white boxed region showing fine structures. **e**, Layer-by-layer approaches: buckyball structures fabricated by projecting 2D patterns into a photoresin and confining the printing process to the image plane via an intersecting thin sheet of light in the image plane. Inset: increased magnification of single buckyball. **f**, Inorganic printing: conductive gold–polymer composite lines formed through simultaneous photoreduction and polymerization by scanning a laser focus inside an aqueous ink. Part **a** adapted with permission from ref. 25, Springer Nature Ltd. Part **b** (right) adapted from ref. 58, CC BY 4.0. Part **b** (left, bottom) adapted with permission from ref. 11, Optica. Part b (left, top) adapted with permission from ref. 24, Optica. Part **c** adapted with permission from ref. 74, CC BY 4.0. Part **d** adapted with permission from ref. 29, CC BY 4.0. Part **e** adapted with permission from ref. 21, Springer Nature Ltd. Part **f** adapted with permission from ref. 159, Wiley.

exposure by light is above D_{th}, a sufficiently solidified polymer remains in the development process[49]. Otherwise, the ink (a monomer) is washed out. Chemically, the deposited exposure dose leads to a certain density of dissociated initiator molecules that trigger a polymerization chain reaction. Initially, this trigger is blocked because quencher molecules such as oxygen dissolved in the ink efficiently capture the initiator fragments. Once the quencher is locally consumed, the polymerization chain reaction starts. It is terminated once the quencher diffuses back into the reaction zone, typically on a timescale of some hundreds of microseconds, as determined by physical in situ experiments[147]. Thereby, the exposure dose is translated into a local cross-linking density of the molecules. If this density of chemical bonds is sufficiently large, the molecules can no longer be washed out in the development process, qualitatively explaining the occurrence of a threshold in the threshold model. In polymer printing on the microscale and nanoscale, local increases of the temperature T are typically unimportant[148], whereas on the macroscale, heating can be a major issue[90].

Noble metals such as gold[149–151], silver[32,152,153] and platinum[138,154] have been laser-printed starting from metal salts dissolved in optically transparent aqueous inks. The local light intensity reduces these salts via one-photon or multi-photon absorption, leading to a distribution of nanoparticles, initially following the deposited dose $D(\mathbf{r}, t)$. These particles can move owing to forces induced by strong local temperature gradients arising from $T(\mathbf{r}, t)$ or by light-induced forces such as the light pressure[155], the optical gradient force[156] and dipole–dipole forces[138,157], all of which are directly connected to $\mathbf{E}(\mathbf{r}, t)$. A part of these nanoparticles is then locally sintered together under the influence of the intense laser irradiation. This process can also be combined with the simultaneous polymerization of a monomer[158–162], leading to improved mechanical stability of the metal–polymer blend (Fig. 4f).

In laser printing of semiconducting metal oxides, such as ZnO (ref. 137), again from optically transparent aqueous inks, the temperature increase described by the profile $T(\mathbf{r}, t)$ induced by a tight focus of light has the key role. It locally starts a thermally activated crystallization process via the Boltzmann factor proportional to $\exp(-E_A/(k_B T(\mathbf{r}, t))$, with activation energy E_A and Boltzmann constant k_B, and is referred to as hydrothermal synthesis[163]. The Boltzmann factor steeply increases as T increases, and hence also as I increases, and thereby again introduces a threshold-like behaviour. Large local temperature increases and subsequent local melting of material are also the basis of well-established and widespread 3D print processes on the macroscale such as selective laser sintering and selective laser melting[53,164]. In these techniques, the laser focus induces melting of solid particles in a powder bed of polymer or metal. In all such thermal processes, one must find a trade-off between achieving sufficiently localized temperature profiles with large peaks (low heat conductivity) and sufficiently short time constants (large heat conductivity).

Finally, many different effective material properties can be achieved by microstructuring an ordinary ingredient material in 3D. The resulting 'metamaterials' can directly be manufactured as part of the 3D print process and can be seen as 'meta-inks'[35,165–167].

Key 3D printing performance parameters

In the Introduction, we pointed out that 2D graphical ink-jet printers presently operate at speeds of around 10^6–10^7 pixels s^{-1} and with pixel sizes down to a few tens of micrometres. At what speeds in units of voxel s^{-1} and at what voxel sizes do today's 3D material printers based on light operate? Figure 5 provides an overview on these two metrics on a double-logarithmic scale, spanning several orders of magnitude for both the voxel size s_{voxel} and the print rate R_{voxel}. In the plot, the data points for interference lithography of periodic 3D nanostructures stand out by far – although they must be taken with a grain of salt as the voxel size (conservatively taken as $s_{voxel} = \lambda/4$) is not strictly defined for this approach and a long post-bake treatment is typically required before polymerization. The wide range of rates results from the fact that interference lithography is a truly volumetric approach in which the entire 3D structure is exposed using timescales of a few seconds[31] to a single intense few-nanosecond-long optical pulse[25]. However, the approach is restricted to periodic architectures. Tomographic volumetric additive manufacturing has yet to fully reach its potential in terms of print speed because many sequential exposures by light are used in practice. In fact, all other approaches in Fig. 4 use sequential exposures in one form or another, and as a result, their speed is limited by engineering issues or by the available power of light. The latter is a physics limitation.

The formation of one voxel of material of a given size s_{voxel} needs a finite absorbed optical energy, say, E_{voxel} (with units $[E_{voxel}] = \mathrm{J\ voxel^{-1}}$). Therefore, the mean laser power P_{laser} required follows

$$P_{laser} = \eta^{-1} E_{voxel}\, R_{voxel}. \tag{13}$$

Herein, the efficiency $\eta \in [0\%, 100\%]$ is a dimensionless constant, describing the fact that only a small fraction of the incident laser light is absorbed (which is fundamental as the ink needs to be sufficiently transparent) and that only a fraction ≤100% of the power P_{laser} emerging from the laser will enter the print zone (Fig. 1). Let us consider an example. Two-photon focus-scanning printing with print rates $R_{voxel} \approx 10^7$ voxel s^{-1} requires mean powers out of a continuously mode-locked femtosecond laser of $P_{laser} \approx 3$ W (hence, $\eta^{-1} E_{voxel} \approx 0.3$ μJ)[58]. Then, the printing of 3×10^{11} voxels requires an optical energy of 90 kJ out of the laser. Therefore, we conclude that, although materials science and improved optics might reduce the necessary $\eta^{-1} E_{voxel}$ in the future, one should be aware that the ultimately accessible print rate for a given ink may be limited by available power from a laser or from other intense light sources. Here, we have considered a light-based perspective. More generally, there is a competition of limits. For example, heating owing to light-induced exothermal chemical processes may impose such a limit[90].

Although Fig. 5 provides a quantitative overview, we note that it only captures two of the key performance parameters of 3D printers. Other relevant key performance parameters are the flexibility in terms of which materials can be 3D printed, the power consumption and the cost of the instrument. For example, the instrument cost varies by several orders of magnitude for the data points in Fig. 5. We are presently unable to collect these key performance parameters systematically and quantitatively from the existing literature. However, we do further address them qualitatively in the following section.

Outlook

Three-dimensional printing with light has already led to numerous applications in photonics[168–170], electronics[171–175], mechanics[176–179], micro-robotics[180–184] and biology[185–188] that would not have been possible along conventional (subtractive) paths of manufacturing. Nevertheless, the pressing challenges of 3D printing continue to be to make it 'finer', that is, to improve the accessible spatial resolution, 'faster', that is, to further boost the print speed in terms of voxel s^{-1}, 'more', that is, to largely expand the possibilities of multi-material printing, and 'less expensive', that is, to bring the cost of high-end 3D printers down from sometimes many hundreds of thousands to perhaps just a few thousand euros or dollars.

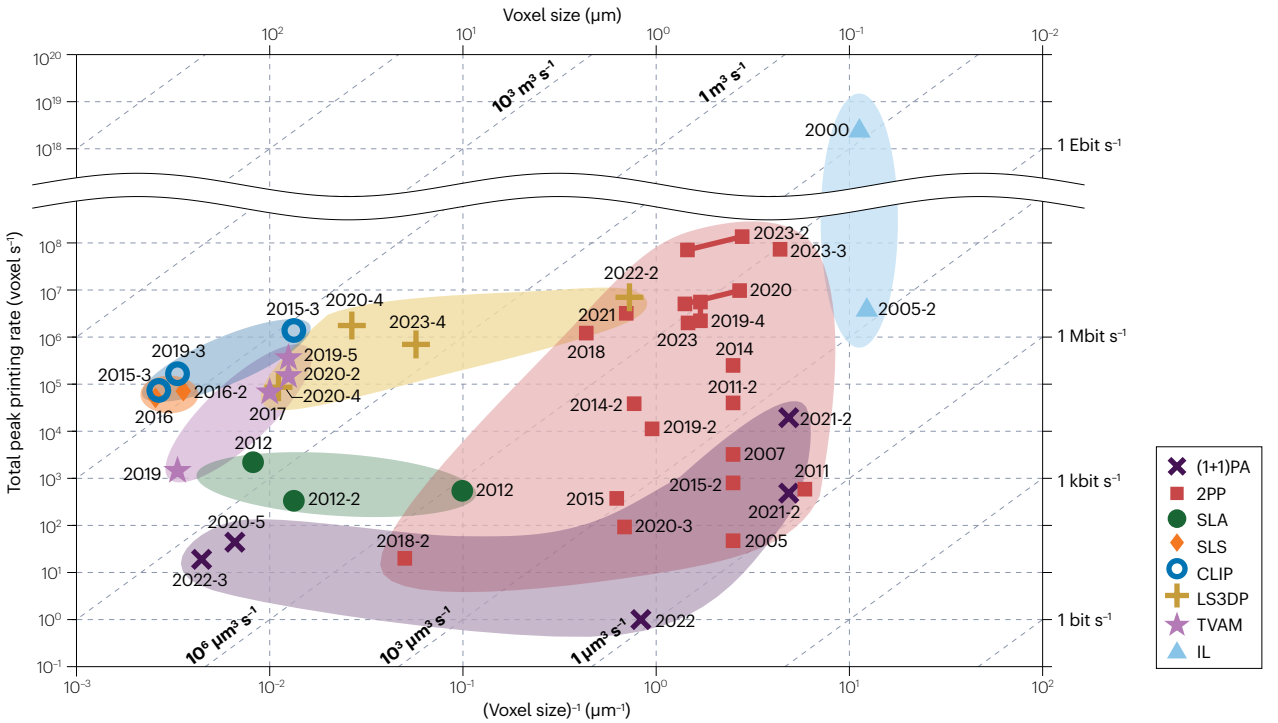

Fig. 5 | Three-dimensional printing speed of various light-based processes. Comparison of the voxel size (taken as an average of the lateral and vertical voxel dimensions)[58] and print rate in voxel s^{-1} of various light-based 3D printing processes. The time taken for pre-processing and post-processing steps is not included in the presented printing rates. Data sources for the data points are as follows: 2000 (ref. 25), 2005 (ref. 191), 2005-1 (ref. 31), 2007 (ref. 192), 2011 (ref. 134), 2011-2 (ref. 193), 2012 (refs. 194–196; data points are from ref. 27), 2012-2 (ref. 197), 2014 (ref. 198), 2014-2 (ref. 199), 2015 (ref. 56), 2015-2 (ref. 200), 2015-3 (ref. 89), 2016 (ref. 201), 2016-2 (ref. 202), 2017 (ref. 27), 2018 (ref. 203), 2018-2 (ref. 75), 2019 (ref. 28), 2019-2 (ref. 57), 2019-3 (ref. 90), 2019-4 (ref. 78), 2019-5 (ref. 185), 2020 (ref. 58), 2020-2 (ref. 29), 2020-3 (ref. 204), 2020-4 (ref. 20; the authors of ref. 20 estimate a voxel size of 37.5 μm, leading to a printing rate of 1.8×10^6 voxel s^{-1}; we rather estimate a voxel size in 3D of 90 μm from the data shown in ref. 20 leading to a printing rate of 8.6×10^4 voxel s^{-1}), 2020-5 (ref. 123), 2021 (ref. 74), 2021-2 (ref. 101), 2022 (ref. 128), 2022-2 (ref. 21), 2022-3 (ref. 125), 2023 (ref. 60), 2023-2 (ref. 61), 2023-3 (ref. 189) and 2023-4 (ref. 205). Figure adapted with permission from ref. 58, CC BY 4.0. (1+1)PA, (1+1)-photon absorption; 2PP, two-photon polymerization; CLIP, continuous liquid interface printing; IL, interference lithography; LS3DP, light-sheet 3D printing; SLA, stereolithography; SLS, selective laser sintering; TVAM, tomographic volumetric additive manufacturing.

Concerning 'finer', STED-inspired approaches have already broken the optical diffraction barrier (the two-photon Sparrow criterion[49]) in 3D printing by a factor of about two in voxel size (factor of eight in voxel volume) – but so far not more, limited by parasitic multi-photon excitation processes. Conceptually, much larger factors are possible, enabling resolutions down to the scale of a few tens of nanometres. Replacing two-photon absorption by two-step absorption in combination with STED appears as a promising future avenue. Such spatial resolutions and precisions are necessary for applications such as 3D printing of micro-optical components for future 3D optical chips or advanced high-quality-factor 3D optical cavities for quantum-optical technologies. For such optical 3D microstructures and nanostructures, there may not be any alternative way of making them besides 3D printing.

With respect to 'faster', 3D printing with light is already used in industry for making masters on the macroscale and microscale. Examples include nanostructured masters for mass-replicating optically smooth free-form surfaces or diffractive optical elements for mobile-phone applications. However, many truly 3D objects just cannot be replicated in that way and must be 3D printed piece-by-piece. In this Review, we have shown that, conceptually, arbitrary complex 3D microstructures can be manufactured in a single volumetric exposure by a single short optical pulse, in perhaps some tens of picoseconds. However, such an ultimate flexible holographic approach has not been realized experimentally so far. As we were writing this Review, multi-focus multi-photon 3D laser nanoprinting sped up by about another order of magnitude to print rates close to 10^8 voxel s^{-1} at deep sub-micrometre voxel sizes[189]. Along these lines, seemingly exotic applications, such as 3D printing-tailored 3D microparticles for pharmacy (by inhalation as envisioned in a review article[190]), come into reach as now literally millions of such particles can be printed within 1 day.

Regarding 'more', the use of material formation and addition mechanisms other than photopolymerization, such as photo-thermal activation of crystal-growth processes from solution, has enabled 3D printing of semiconductors and metals for functional microelectronics[137] and bioelectronics. Here, the door is wide open and new materials options appear seemingly weekly. To further expand the materials options, it is also conceivable to replace liquid inks by gaseous precursors.

Finally, concerning 'less expensive', 3D laser microprinters and nanoprinters have already entered multi-user shared clean room facilities at many academic institutions around the globe. Although numbers will probably increase in the years to come, costs in the range of hundreds of thousands of euros or dollars are prohibitive for many small university groups. Various new forms of (1+1)-photon absorption[130]

have just recently opened the door to a new generation of instruments that operate with pinhead-sized semiconductor continuous-wave lasers at light power levels below 1 mW. These semiconductor lasers cost only several tens of euros or dollars in contrast to tens to hundreds of thousands of euros or dollars for currently utilized pulsed laser systems, while simultaneously also only being a fraction of the size. The drastic miniaturization of the rest of the 3D printer is subject of active research and commercialization efforts.

We expect that, in achieving all these perspectives for 3D printing, physics will have a key role. However, physics still needs to be intimately intertwined with optical science, laser science, chemistry, materials science and the engineering sciences.

Data availability

A maintained and updated version of Fig. 5 is provided at https://3DprintingSpeed.com.

Published online: 12 December 2023

References

1. Gottwald, J. F. Liquid metal recorder. US Patent US3596285A (1971).
2. Sachs, E. M., Haggerty, J. S., Cima, M. J. & Williams, P. A. Three-dimensional printing techniques. US Patent US5204055A (1993).
3. de Gans, B. J., Duineveld, P. C. & Schubert, U. S. Inkjet printing of polymers: state of the art and future developments. *Adv. Mater.* **16**, 203–213 (2004).
4. Delrot, P., Modestino, M. A., Gallaire, F., Psaltis, D. & Moser, C. Inkjet printing of viscous monodisperse microdroplets by laser-induced flow focusing. *Phys. Rev. Appl.* **6**, 024003 (2016).
5. Crump, S. S. Apparatus and method for creating three-dimensional objects. US Patent US5121329A (1992).
6. Landauer, R. Light faster than light? *Nature* **365**, 692–693 (1993).
7. Hell, S. W. & Wichmann, J. Breaking the diffraction resolution limit by stimulated emission: stimulated-emission-depletion fluorescence microscopy. *Opt. Lett.* **19**, 780 (1994).
8. Klar, T. A., Jakobs, S., Dyba, M., Egner, A. & Hell, S. W. Fluorescence microscopy with diffraction resolution barrier broken by stimulated emission. *Proc. Natl Acad. Sci. USA* **97**, 8206–8210 (2000).
9. Hell, S. W. Strategy for far-field optical imaging and writing without diffraction limit. *Phys. Lett. A* **326**, 140–145 (2004).
10. Thiel, M., Ott, J., Radke, A., Kaschke, J. & Wegener, M. Dip-in depletion optical lithography of three-dimensional chiral polarizers. *Opt. Lett.* **38**, 4252 (2013).
11. Kaschke, J. & Wegener, M. Gold triple-helix mid-infrared metamaterial by STED-inspired laser lithography. *Opt. Lett.* **40**, 3986 (2015).
12. Fischer, J. et al. Exploring the mechanisms in STED-enhanced direct laser writing. *Adv. Opt. Mater.* **3**, 221–232 (2015).
13. Müller, P. et al. STED-inspired laser lithography based on photoswitchable spirothiopyran moieties. *Chem. Mater.* **31**, 1966–1972 (2019).
14. Liaros, N. & Fourkas, J. T. Ten years of two-color photolithography [Invited]. *Opt. Mater. Express* **9**, 3006 (2019).
15. He, M. et al. 3D sub-diffraction printing by multicolor photoinhibition lithography: from optics to chemistry. *Laser Photon Rev.* **16**, 2100229 (2022).
16. Somers, P. et al. Photo-activated polymerization inhibition process in photoinitiator systems for high-throughput 3D nanoprinting. *Nanophotonics* https://doi.org/10.1515/NANOPH-2022-0611 (2023).
17. Jones, D. E. H. Ariadne. *New Scientist*. 80 (1974).
18. Swainson, W. K. Method, medium and apparatus for producing three-dimensional figure product. US Patent US4041476A (1971).
19. Ford, J. E. et al. in *Photonics for Processors, Neural Networks, and Memories* Vol. 2026 (eds Horner, J. L. et al.) 604–613 (SPIE, 1993).
20. Regehly, M. et al. Xolography for linear volumetric 3D printing. *Nature* **588**, 620–624 (2020).
21. Hahn, V. et al. Light-sheet 3D microprinting via two-colour two-step absorption. *Nat. Photonics* **16**, 784–791 (2022).
22. Kodama, H. Automatic method for fabricating a three-dimensional plastic model with photo-hardening polymer. *Rev. Sci. Instrum.* **52**, 1770–1773 (1981).
23. Hull, C. W. Apparatus for production of three-dimensional objects by stereolithography. US Patent US4575330A (1986).
24. Maruo, S., Nakamura, O. & Kawata, S. Three-dimensional microfabrication with two-photon-absorbed photopolymerization. *Opt. Lett.* **22**, 132 (1997).
25. Campbell, M., Sharp, D. N., Harrison, M. T., Denning, R. G. & Turberfield, A. J. Fabrication of photonic crystals for the visible spectrum by holographic lithography. *Nature* **404**, 53–56 (2000).
26. Wu, X. Imaging and forming method using projection operation and back projection method. European Patent EP3333629A4 (2016).
27. Shusteff, M. et al. One-step volumetric additive manufacturing of complex polymer structures. *Sci. Adv.* **3**, eaao5496 (2017).
28. Kelly, B. E. et al. Volumetric additive manufacturing via tomographic reconstruction. *Science* **363**, 1075–1079 (2019).
29. Loterie, D., Delrot, P. & Moser, C. High-resolution tomographic volumetric additive manufacturing. *Nat. Commun.* **11**, 852 (2020).
30. Melde, K. et al. Compact holographic sound fields enable rapid one-step assembly of matter in 3D. *Sci. Adv.* **9**, eadf6182 (2023).
31. Pang, Y. K. et al. Chiral microstructures (spirals) fabrication by holographic lithography. *Opt. Express* **13**, 7615 (2005).
32. Liu, L. et al. Fast fabrication of silver helical metamaterial with single-exposure femtosecond laser photoreduction. *Nanophotonics* **8**, 1087–1093 (2019).
33. Cai, L. Z., Yang, X. L. & Wang, Y. R. All fourteen Bravais lattices can be formed by interference of four noncoplanar beams. *Opt. Lett.* **27**, 900 (2002).
34. Meisel, D. C., Wegener, M. & Busch, K. Three-dimensional photonic crystals by holographic lithography using the umbrella configuration: symmetries and complete photonic band gaps. *Phys. Rev. B Condens. Matter Mater. Phys.* **70**, 165104 (2004).
35. Kadic, M., Milton, G. W., van Hecke, M. & Wegener, M. 3D metamaterials. *Nat. Rev. Phys.* **1**, 198–210 (2019).
36. Feth, N., Enkrich, C., Wegener, M. & Linden, S. Large-area magnetic metamaterials via compact interference lithography. *Opt. Express* **15**, 501 (2007).
37. Behera, S. & Joseph, J. Design and realization of functional metamaterial basis structures through optical phase manipulation based interference lithography. *J. Opt.* **19**, 105103 (2017).
38. Miklyaev, Y. V. et al. Three-dimensional face-centered-cubic photonic crystal templates by laser holography: fabrication, optical characterization, and band-structure calculations. *Appl. Phys. Lett.* **82**, 1284–1286 (2003).
39. Divliansky, I., Mayer, T. S., Holliday, K. S. & Crespi, V. H. Fabrication of three-dimensional polymer photonic crystal structures using single diffraction element interference lithography. *Appl. Phys. Lett.* **82**, 1667–1669 (2003).
40. Wu, L., Zhong, Y., Chan, C. T., Wong, K. S. & Wang, G. P. Fabrication of large area two- and three-dimensional polymer photonic crystals using single refracting prism holographic lithography. *Appl. Phys. Lett.* **86**, 241102 (2005).
41. Frenzel, T., Kadic, M. & Wegener, M. Three-dimensional mechanical metamaterials with a twist. *Science* **358**, 1072–1074 (2017).
42. Ullal, C. K. et al. Photonic crystals through holographic lithography: simple cubic, diamond-like, and gyroid-like structures. *Appl. Phys. Lett.* **84**, 5434–5436 (2004).
43. Leibovici, M. C. R. & Gaylord, T. K. Photonic-crystal waveguide structure by pattern-integrated interference lithography. *Opt. Lett.* **40**, 2806 (2015).
44. Leibovici, M. C. R. & Gaylord, T. K. Custom-modified three-dimensional periodic microstructures by pattern-integrated interference lithography. *J. Opt. Soc. Am. A* **31**, 1515 (2014).
45. Ohlinger, K., Lutkenhaus, J., Arigong, B., Zhang, H. & Lin, Y. Spatially addressable design of gradient index structures through spatial light modulator based holographic lithography. *J. Appl. Phys.* https://doi.org/10.1063/1.4837635 (2013).
46. Wolf, E. Electromagnetic diffraction in optical systems — I. An integral representation of the image field. *Proc. R. Soc. Lond. A Math. Phys. Sci.* **253**, 349–357 (1959).
47. Abbe, E. Beiträge zur theorie des mikroskops und der mikroskopischen wahrnehmung. *Arch. für Mikrosk. Anat.* **9**, 413–468 (1873).
48. Gu, M. & Sheppard, C. J. R. Comparison of three-dimensional imaging properties between two-photon and single-photon fluorescence microscopy. *J. Microsc.* **177**, 128–137 (1995).
49. Fischer, J. & Wegener, M. Three-dimensional optical laser lithography beyond the diffraction limit. *Laser Photon Rev.* **7**, 22–44 (2013).
50. Wong, S. et al. Direct laser writing of three-dimensional photonic crystals with a complete photonic band gap in chalcogenide glasses. *Adv. Mater.* **18**, 265–269 (2006).
51. Williams, H. E., Luo, Z. & Kuebler, S. M. Effect of refractive index mismatch on multi-photon direct laser writing. *Opt. Express* **20**, 25030 (2012).
52. Deckard, C. Method and apparatus for producing parts by selective sintering. US Patent US4863538A (1989).
53. Gu, D. D., Meiners, W., Wissenbach, K. & Poprawe, R. Laser additive manufacturing of metallic components: materials, processes and mechanisms. *Int. Mater. Rev.* **57**, 133–164 (2012).
54. Matsuo, S., Juodkazis, S. & Misawa, H. Femtosecond laser microfabrication of periodic structures using a microlens array. *Appl. Phys. A* **80**, 683–685 (2005).
55. Obata, K. et al. Multi-focus two-photon polymerization technique based on individually controlled phase modulation. *Opt. Express* **18**, 17193–17200 (2010).
56. Yang, L. et al. Parallel direct laser writing of micro-optical and photonic structures using spatial light modulator. *Opt. Lasers Eng.* **70**, 26–32 (2015).
57. Geng, Q., Wang, D., Chen, P. & Chen, S. C. Ultrafast multi-focus 3-D nano-fabrication based on two-photon polymerization. *Nat. Commun.* https://doi.org/10.1038/s41467-019-10249-2 (2019).
58. Hahn, V. et al. Rapid assembly of small materials building blocks (voxels) into large functional 3D metamaterials. *Adv. Funct. Mater.* **30**, 1907795 (2020).
59. Manousidaki, M., Papazoglou, D. G., Farsari, M. & Tzortzakis, S. 3D holographic light shaping for advanced multiphoton polymerization. *Opt. Lett.* **45**, 85 (2020).
60. Ouyang, W. et al. Ultrafast 3D nanofabrication via digital holography. *Nat. Commun.* **14**, 1716 (2023).
61. Kiefer, P. et al. A multi-photon (7×7)-focus 3D laser printer based on a 3D-printed diffractive optical element and a 3D-printed multi-lens array. *Light Adv. Manuf.* (in the press).

62. Keller, J., Schönle, A. & Hell, S. W. Efficient fluorescence inhibition patterns for RESOLFT microscopy. *Opt. Express* **15**, 3361 (2007).
63. Arlt, J. & Padgett, M. J. Generation of a beam with a dark focus surrounded by regions of higher intensity: the optical bottle beam. *Opt. Lett.* **25**, 191 (2000).
64. Zhang, S. J. et al. Two-photon polymerization of a three dimensional structure using beams with orbital angular momentum. *Appl. Phys. Lett.* **105**, 061101 (2014).
65. Tang, J., Ren, J. & Han, K. Y. Fluorescence imaging with tailored light. *Nanophotonics* **8**, 2111–2128 (2019).
66. Gerchberg, R. W. & Saxton, W. O. A practical algorithm for the determination of phase from image and diffraction plane pictures. *Optik* **35**, 237–246 (1972).
67. Haist, T., Schönleber, M. & Tiziani, H. J. Computer-generated holograms from 3D-objects written on twisted-nematic liquid crystal displays. *Opt. Commun.* **140**, 299–308 (1997).
68. Yang, L. et al. Projection two-photon polymerization using a spatial light modulator. *Opt. Commun.* **331**, 82–86 (2014).
69. Yang, L. et al. Two-photon polymerization of microstructures by a non-diffraction multifoci pattern generated from a superposed Bessel beam. *Opt. Lett.* **42**, 743 (2017).
70. Yang, D., Liu, L., Gong, Q. & Li, Y. Rapid two-photon polymerization of an arbitrary 3D microstructure with 3D focal field engineering. *Macromol. Rapid Commun.* **40**, 1900041 (2019).
71. Durfee, C. G., Greco, M., Block, E., Vitek, D. & Squier, J. A. Intuitive analysis of space-time focusing with double-ABCD calculation. *Opt. Express* **20**, 14244 (2012).
72. Oron, D., Tal, E. & Silberberg, Y. Scanningless depth-resolved microscopy. *Opt. Express* **13**, 1468 (2005).
73. Zhu, G., van Howe, J., Durst, M., Zipfel, W. & Xu, C. Simultaneous spatial and temporal focusing of femtosecond pulses. *Opt. Express* **13**, 2153 (2005).
74. Somers, P. et al. Rapid, continuous projection multi-photon 3D printing enabled by spatiotemporal focusing of femtosecond pulses. *Light Sci. Appl.* **10**, 199 (2021).
75. Chu, W. et al. Centimeter-height 3D printing with femtosecond laser two-photon polymerization. *Adv. Mater. Technol.* **3**, 1700396 (2018).
76. Kim, D. & So, P. T. C. High-throughput three-dimensional lithographic microfabrication. *Opt. Lett.* **35**, 1602 (2010).
77. Li, Y.-C. et al. Fast multiphoton microfabrication of freeform polymer microstructures by spatiotemporal focusing and patterned excitation. *Opt. Express* **20**, 19030 (2012).
78. Saha, S. K. et al. Scalable submicrometer additive manufacturing. *Science* **366**, 105–109 (2019).
79. Sun, B. et al. Four-dimensional light shaping: manipulating ultrafast spatiotemporal foci in space and time. *Light Sci. Appl.* **7**, 17117 (2017).
80. Dinc, N. U. et al. From 3D to 2D and back again. *Nanophotonics* https://doi.org/10.1515/nanoph-2022-0512 (2023).
81. Radon, J. On the determination of functions from their integral values along certain manifolds. *IEEE Trans. Med. Imaging* **5**, 170–176 (1986).
82. Bhattacharya, I., Toombs, J. & Taylor, H. High fidelity volumetric additive manufacturing. *Addit. Manuf.* **47**, 102299 (2021).
83. Rackson, C. M. et al. Object-space optimization of tomographic reconstructions for additive manufacturing. *Addit. Manuf.* **48**, 102367 (2021).
84. Madrid-Wolff, J., Boniface, A., Loterie, D., Delrot, P. & Moser, C. Controlling light in scattering materials for volumetric additive manufacturing. *Adv. Sci.* **9**, 2105144 (2022).
85. Bertsch, A., Jézéquel, J. Y. & André, J. C. Study of the spatial resolution of a new 3D microfabrication process: the microstereophotolithography using a dynamic mask-generator technique. *J. Photochem. Photobiol. A Chem.* **107**, 275–281 (1997).
86. Sun, C., Fang, N., Wu, D. M. & Zhang, X. Projection micro-stereolithography using digital micro-mirror dynamic mask. *Sens. Actuators A Phys.* **121**, 113–120 (2005).
87. Huang, Y. M. & Jiang, C. P. On-line force monitoring of platform ascending rapid prototyping system. *J. Mater. Process. Technol.* **159**, 257–264 (2005).
88. Jin, J., Yang, J., Mao, H. & Chen, Y. A vibration-assisted method to reduce separation force for stereolithography. *J. Manuf. Process.* **34**, 793–801 (2018).
89. Tumbleston, J. R. et al. Continuous liquid interface production of 3D objects. *Science* **347**, 1349–1352 (2015).
90. Walker, D. A., Hedrick, J. L. & Mirkin, C. A. Rapid, large-volume, thermally controlled 3D printing using a mobile liquid interface. *Science* **366**, 360–364 (2019).
91. De Beer, M. P. et al. Rapid, continuous additive manufacturing by volumetric polymerization inhibition patterning. *Sci. Adv.* **5**, eaau8723 (2019).
92. Anandakrishnan, N. et al. Fast stereolithography printing of large-scale biocompatible hydrogel models. *Adv. Healthc. Mater.* **10**, 2002103 (2020).
93. Mueller, P., Thiel, M. & Wegener, M. 3D direct laser writing using a 405 nm diode laser. *Opt. Lett.* **39**, 6847 (2014).
94. Wickberg, A. et al. Second-harmonic generation by 3D laminate metacrystals. *Adv. Opt. Mater.* **7**, 1801235 (2019).
95. Sanli, U. T. et al. High-resolution kinoform X-ray optics printed via 405 nm 3D laser lithography. *Adv. Mater. Technol.* **7**, 2101695 (2022).
96. Wang, H. et al. Two-photon polymerization lithography for optics and photonics: fundamentals, materials, technologies, and applications. *Adv. Funct. Mater* https://doi.org/10.1002/adfm.202214211 (2023).
97. Dirac, P. A. M. The quantum theory of the emission and absorption of radiation. *Proc. R. Soc. Lond. Ser. A* **114**, 243–265 (1927).
98. Schäfer, W. & Wegener, M. Interaction of Matter and Electromagnetic Fields. In: *Semiconductor Optics and Transport Phenomena. Advanced Texts in Physics*. 7–49 (Springer, 2002).
99. Poynting, J. H. X. V. On the transfer of energy in the electromagnetic field. *Philos. Trans. R. Soc. Lond.* **175**, 343–361 (1884).
100. Mauri, A. et al. Two- and three-photon processes in photoinitiators for 3D laser printing. Preprint at *Res. Sq.* https://doi.org/10.21203/rs.3.rs-1797484/v1 (2022).
101. Hahn, V. et al. Two-step absorption instead of two-photon absorption in 3D nanoprinting. *Nat. Photonics* **15**, 932–938 (2021).
102. Liaros, N. et al. Elucidating complex triplet-state dynamics in the model system isopropylthioxanthone. *iScience* **25**, 103600 (2022).
103. Yang, L. et al. On the Schwarzschild effect in 3D two-photon laser lithography. *Adv. Opt. Mater.* **7**, 1901040 (2019).
104. Johnson, J. E., Chen, Y. & Xu, X. Model for polymerization and self-deactivation in two-photon nanolithography. *Opt. Express* **30**, 26824 (2022).
105. Kiefer, P. et al. Sensitive photoresists for rapid multiphoton 3D laser micro- and nanoprinting. *Adv. Opt. Mater.* **8**, 2000895 (2020).
106. Kawata, S., Sun, H.-B., Tanaka, T. & Takada, K. Finer features for functional microdevices. *Nature* **412**, 697–698 (2001).
107. Göppert-Mayer, M. Über elementarakte mit zwei quantensprüngen. *Ann. Phys.* **401**, 273–294 (1931).
108. Strickler, J. H. & Webb, W. W. in *CAN-AM Eastern '90* Vol. 1398 (eds Antos, R. L. & Krisiloff, A. J.) 107–118 (SPIE, 1991).
109. Boyd, R. W. *Nonlinear Optics* (Academic, 2008).
110. Pucher, N. et al. Structure-activity relationship in D-π-a-π-D-based photoinitiators for the two-photon-induced photopolymerization process. *Macromolecules* **42**, 6519–6528 (2009).
111. Li, Z. et al. A straightforward synthesis and structure-activity relationship of highly efficient initiators for two-photon polymerization. *Macromolecules* **46**, 352–361 (2013).
112. Nazir, R. et al. Donor-acceptor type thioxanthones: synthesis, optical properties, and two-photon induced polymerization. *Macromolecules* **48**, 2466–2472 (2015).
113. Chi, T. et al. Substituted thioxanthone-based photoinitiators for efficient two-photon direct laser writing polymerization with two-color resolution. *ACS Appl. Polym. Mater.* **3**, 1426–1435 (2021).
114. Ladika, D. et al. Synthesis and application of triphenylamine-based aldehydes as photo-initiators for multi-photon lithography. *Appl. Phys. A Mater. Sci. Process.* **128**, (2022).
115. Lunzer, M. et al. Beyond the threshold: a study of chalcogenophene-based two-photon initiators. *Chem. Mater.* **34**, 3042–3052 (2022).
116. Fischer, J. et al. Three-dimensional multi-photon direct laser writing with variable repetition rate. *Opt. Express* **21**, 26244 (2013).
117. Tomova, Z., Liaros, N., Gutierrez Razo, S. A., Wolf, S. M. & Fourkas, J. T. In situ measurement of the effective nonlinear absorption order in multiphoton photoresists. *Laser Photon Rev.* **10**, 849–854 (2016).
118. Maruo, S. & Ikuta, K. Three-dimensional microfabrication by use of single-photon-absorbed polymerization. *Appl. Phys. Lett.* **76**, 2656–2658 (2000).
119. Delrot, P., Loterie, D., Psaltis, D. & Moser, C. Single-photon three-dimensional microfabrication through a multimode optical fiber. *Opt. Express* **26**, 1766 (2018).
120. Hsu, S. et al. High-speed one-photon 3D nanolithography using controlled initiator depletion and inhibitor transport. *Adv. Opt. Mater.* **10**, 2102262 (2022).
121. Bojanowski, N. M. et al. Search for alternative two-step-absorption photoinitiators for 3D laser nanoprinting. *Adv. Funct. Mater.* **33**, 2212482 (2022).
122. Rocheva, V. V. et al. High-resolution 3D photopolymerization assisted by upconversion nanoparticles for rapid prototyping applications. *Sci. Rep.* **8**, 3663 (2018).
123. Chen, Y. et al. Noninvasive in vivo 3D bioprinting. *Sci. Adv.* **6**, eba7406 (2020).
124. Zhu, J., Zhang, Q., Yang, T., Liu, Y. & Liu, R. 3D printing of multi-scalable structures via high penetration near-infrared photopolymerization. *Nat. Commun.* **11**, 3462 (2020).
125. Sanders, S. N. et al. Triplet fusion upconversion nanocapsules for volumetric 3D printing. *Nature* **604**, 474–478 (2022).
126. Zhang, Q., Boniface, A., Parashar, V. K., Gijs, M. A. M. & Moser, C. Multi-photon polymerization using upconversion nanoparticles for tunable feature-size printing. *Nanophotonics* https://doi.org/10.1515/nanoph-2022-0598 (2023).
127. Schloemer, T. et al. Nanoengineering triplet–triplet annihilation upconversion: from materials to real-world applications. *ACS Nano* **17**, 3259–3288 (2023).
128. Limberg, D. K., Kang, J. H. & Hayward, R. C. Triplet-triplet annihilation photopolymerization for high-resolution 3D printing. *J. Am. Chem. Soc.* **144**, 5226–5232 (2022).
129. Luo, Z. et al. Three-dimensional nanolithography with visible continuous wave laser through triplet up-conversion. *J. Phys. Chem. Lett.* **14**, 709–715 (2023).
130. Hahn, V. et al. Challenges and opportunities in 3D laser printing based on (1 + 1)-photon absorption. *ACS Photonics* **10**, 24–33 (2023).
131. Samsonas, D. et al. 3D nanopolymerization and damage threshold dependence on laser wavelength and pulse duration. *Nanophotonics* https://doi.org/10.1515/nanoph-2022-0629 (2023).
132. Denk, W., Strickler, J. H. & Webb, W. W. Two-photon laser scanning fluorescence microscopy. *Science* **248**, 73–76 (1990).
133. Li, L., Gattass, R. R., Gershgoren, E., Hwang, H. & Fourkas, J. T. Achieving λ/20 resolution by one-color initiation and deactivation of polymerization. *Science* **324**, 910–913 (2009).
134. Fischer, J. & Wegener, M. Three-dimensional direct laser writing inspired by stimulated-emission-depletion microscopy [Invited]. *Opt. Mater. Express* **1**, 614 (2011).
135. Wollhofen, R., Katzmann, J., Hrelescu, C., Jacak, J. & Klar, T. A. 120 nm resolution and 55 nm structure size in STED-lithography. *Opt. Express* **21**, 10831 (2013).

136. Fang, T.-S., Brown, R. E., Kwan, C. L. & Singer, L. A. Photophysical studies on benzil. Time resolution of the prompt and delayed emissions and a photokinetic study indicating deactivation of the triplet by reversible exciplex formation. *J. Phys. Chem.* **82**, 2489–2496 (1978).
137. Yang, L. et al. Laser printed microelectronics. *Nat. Commun.* **14**, 1103 (2023).
138. Yang, L. et al. In situ diagnostics and role of light-induced forces in metal laser nanoprinting. *Laser Photon. Rev.* **16**, 2100411 (2022).
139. Tabrizi, S., Cao, Y. Y., Lin, H. & Jia, B. H. Two-photon reduction: a cost-effective method for fabrication of functional metallic nanostructures. *Sci. China Phys. Mech. Astron.* **60**, 034201 (2017).
140. Spiegel, C. A. et al. 4D printing at the microscale. *Adv. Funct. Mater.* **30**, 1907615 (2020).
141. Lay, C. L. et al. Two-photon-assisted polymerization and reduction: emerging formulations and applications. *ACS Appl. Mater. Interfaces* **12**, 10061–10079 (2020).
142. Hobich, J., Blasco, E., Wegener, M., Mutlu, H. & Barner-Kowollik, C. Synergistic, orthogonal, and antagonistic photochemistry for light-induced 3D printing. *Macromol. Chem. Phys.* **224**, 2200318 (2022).
143. Kowsari, K., Akbari, S., Wang, D., Fang, N. X. & Ge, Q. High-efficiency high-resolution multimaterial fabrication for digital light processing-based three-dimensional printing. *3D Print. Addit. Manuf.* **5**, 185–193 (2018).
144. Mayer, F. et al. Multimaterial 3D laser microprinting using an integrated microfluidic system. *Sci. Adv.* **5**, eaau9160 (2019).
145. Maruyama, T., Hirata, H., Furukawa, T. & Maruo, S. Multi-material microstereolithography using a palette with multicolor photocurable resins. *Opt. Mater. Express* **10**, 2522 (2020).
146. Yang, L., Mayer, F., Bunz, U. H. F., Blasco, E. & Wegener, M. Multi-material multi-photon 3D laser micro- and nanoprinting. *Light Adv. Manuf.* **2**, 1 (2021).
147. Mueller, J. B., Fischer, J., Mayer, F., Kadic, M. & Wegener, M. Polymerization kinetics in three-dimensional direct laser writing. *Adv. Mater.* **26**, 6566–6571 (2014).
148. Mueller, J. B., Fischer, J., Mange, Y. J., Nann, T. & Wegener, M. In-situ local temperature measurement during three-dimensional direct laser writing. *Appl. Phys. Lett.* **103**, 123107 (2013).
149. Cao, Y. Y., Takeyasu, N., Tanaka, T., Duan, X. M. & Kawata, S. 3D metallic nanostructure fabrication by surfactant-assisted multiphoton-induced reduction. *Small* **5**, 1144–1148 (2009).
150. Lu, W.-E. et al. Femtosecond direct laser writing of gold nanostructures by ionic liquid assisted multiphoton photoreduction. *Opt. Mater. Express* **3**, 1660 (2013).
151. Lee, M. R. et al. Direct metal writing and precise positioning of gold nanoparticles within microfluidic channels for SERS sensing of gaseous analytes. *ACS Appl. Mater. Interfaces* **9**, 39584–39593 (2017).
152. Komori, T., Furukawa, T., Iijima, M. & Maruo, S. Multi-scale laser direct writing of conductive metal microstructures using a 405-nm blue laser. *Opt. Express* **28**, 8363 (2020).
153. Barton, P. et al. Fabrication of silver nanostructures using femtosecond laser-induced photoreduction. *Nanotechnology* **28**, 505302 (2017).
154. Zarzar, L. D. et al. Multiphoton lithography of nanocrystalline platinum and palladium for site-specific catalysis in 3D microenvironments. *J. Am. Chem. Soc.* **134**, 4007–4010 (2012).
155. Ashkin, A. Acceleration and trapping of particles by radiation pressure. *Phys. Rev. Lett.* **24**, 156–159 (1970).
156. Ashkin, A., Dziedzic, J. M., Bjorkholm, J. E. & Chu, S. Observation of a single-beam gradient force optical trap for dielectric particles. *Opt. Lett.* **11**, 288 (1986).
157. Mie, G. Beiträge zur optik trüber medien, speziell kolloidaler metallösungen. *Ann. Phys.* **330**, 377–445 (1908).
158. Maruo, S. & Saeki, T. Femtosecond laser direct writing of metallic microstructures by photoreduction of silver nitrate in a polymer matrix. *Opt. Express* **16**, 1174 (2008).
159. Blasco, E. et al. Fabrication of conductive 3D gold-containing microstructures via direct laser writing. *Adv. Mater.* **28**, 3592–3595 (2016).
160. Vyatskikh, A. et al. Additive manufacturing of 3D nano-architected metals. *Nat. Commun.* https://doi.org/10.1038/s41467-018-03071-9 (2018).
161. Shukla, S., Furlani, E. P., Vidal, X., Swihart, M. T. & Prasad, P. N. Two-photon lithography of sub-wavelength metallic structures in a polymer matrix. *Adv. Mater.* **22**, 3695–3699 (2010).
162. Shukla, S. et al. Subwavelength direct laser patterning of conductive gold nanostructures by simultaneous photopolymerization and photoreduction. *ACS Nano* **5**, 1947–1957 (2011).
163. Yeo, J. et al. Rapid, one-step, digital selective growth of ZnO nanowires on 3D structures using laser induced hydrothermal growth. *Adv. Funct. Mater.* **23**, 3316–3323 (2013).
164. Farrell, J. et al. Advances in selective laser sintering of polymers. *Int. J. Extrem. Manuf.* **4**, 042002 (2022).
165. Qu, J., Kadic, M., Naber, A. & Wegener, M. Micro-structured two-component 3D metamaterials with negative thermal-expansion coefficient from positive constituents. *Sci. Rep.* **7**, 40643 (2017).
166. Münchinger, A., Hsu, L. Y., Fürniß, F., Blasco, E. & Wegener, M. 3D optomechanical metamaterials. *Mater. Today* **59**, 9–17 (2022).
167. Groß, M. F. et al. Tetramode metamaterials as phonon polarizers. *Adv. Mater.* **35**, e2211801 (2023).
168. Žukauskas, A. et al. Tuning the refractive index in 3D direct laser writing lithography: towards GRIN microoptics. *Laser Photon. Rev.* **9**, 706–712 (2015).
169. Gissibl, T., Thiele, S., Herkommer, A. & Giessen, H. Two-photon direct laser writing of ultracompact multi-lens objectives. *Nat. Photonics* **10**, 554–560 (2016).
170. Liu, Y. et al. Structural color three-dimensional printing by shrinking photonic crystals. *Nat. Commun.* **10**, 4340 (2019).
171. Kiyan, R., Bagratashvili, V. N., Kurselis, K., Popov, V. K. & Chichkov, B. N. 3D fabrication of all-polymer conductive microstructures by two photon polymerization. *Opt. Express* **21**, 31029–31035 (2013).
172. Li, J. et al. Hybrid additive manufacturing of 3D electronic systems. *J. Micromech. Microeng.* **26**, 105005 (2016).
173. Mu, Q. et al. Digital light processing 3D printing of conductive complex structures. *Addit. Manuf.* **18**, 74–83 (2017).
174. Qian, D. et al. Flexible and rapid fabrication of silver microheaters with spatial-modulated multifoci by femtosecond laser multiphoton reduction. *Opt. Lett.* **43**, 5335 (2018).
175. Takenouchi, M., Mukai, M., Furukawa, T. & Maruo, S. Fabrication of flexible wiring with intrinsically conducting polymers using blue-laser microstereolithography. *Polymers* **14**, 4949 (2022).
176. Meza, L. R., Das, S. & Greer, J. R. Strong, lightweight, and recoverable three-dimensional ceramic nanolattices. *Science* **345**, 1322–1326 (2014).
177. Frenzel, T., Findeisen, C., Kadic, M., Gumbsch, P. & Wegener, M. Tailored buckling microlattices as reusable light-weight shock absorbers. *Adv. Mater.* **28**, 5865–5870 (2016).
178. Bauer, J. et al. Nanolattices: an emerging class of mechanical metamaterials. *Adv. Mater.* **29**, 1701850 (2017).
179. Elliott, L. V., Salzman, E. E. & Greer, J. R. Stimuli responsive shape memory microarchitectures. *Adv. Funct. Mater.* **31**, 2008380 (2021).
180. Maruo, S. & Inoue, H. Optically driven viscous micropump using a rotating microdisk. *Appl. Phys. Lett.* **91**, 084101 (2007).
181. Zeng, H. et al. Light-fueled microscopic walkers. *Adv. Mater.* **27**, 3883–3887 (2015).
182. Huang, T.-Y. et al. 3D printed microtransporters: compound micromachines for spatiotemporally controlled delivery of therapeutic agents. *Adv. Mater.* **27**, 6644–6650 (2015).
183. Wang, X. et al. 3D printed enzymatically biodegradable soft helical microswimmers. *Adv. Funct. Mater.* **28**, 1804107 (2018).
184. Ma, Z.-C. et al. Femtosecond laser programmed artificial musculoskeletal systems. *Nat. Commun.* **11**, 4536 (2020).
185. Nuñez Bernal, P. et al. Volumetric bioprinting of complex living-tissue constructs within seconds. *Adv. Mater.* **31**, 1904209 (2019).
186. Hippler, M. et al. 3D scaffolds to study basic cell biology. *Adv. Mater.* **31**, e1808110 (2019).
187. Kozaki, S. et al. Additive manufacturing of micromanipulator mounted on a glass capillary for biological applications. *Micromachines* **11**, 174 (2020).
188. Bernal, P. N. et al. Volumetric bioprinting of organoids and optically tuned hydrogels to build liver-like metabolic biofactories. *Adv. Mater.* **34**, 2110054 (2022).
189. Jiao, B. J. et al. Acousto-optic scanning spatial-switching multiphoton lithography. *Int. J. Extrem. Manuf.* **5**, 035008 (2023).
190. Bock, S., Rades, T., Rantanen, J. & Scherließ, R. Additive manufacturing in respiratory sciences — current applications and future prospects. *Adv. Drug Deliv. Rev.* **186**, 114341 (2022).
191. Kato, J., Takeyasu, N., Adachi, Y., Sun, H.-B. & Kawata, S. Multiple-spot parallel processing for laser micronanofabrication. *Appl. Phys. Lett.* **86**, 044102 (2005).
192. Dong, X. Z., Zhao, Z. S. & Duan, X. M. Micronanofabrication of assembled three-dimensional microstructures by designable multiple beams multiphoton processing. *Appl. Phys. Lett.* **91**, 124103 (2007).
193. Gittard, S. D. et al. Fabrication of microscale medical devices by two-photon polymerization with multiple foci via a spatial light modulator. *Biomed. Opt. Express* **2**, 3167 (2011).
194. Zheng, X. et al. Design and optimization of a light-emitting diode projection micro-stereolithography three-dimensional manufacturing system. *Rev. Sci. Instrum.* **83**, 125001 (2012).
195. Zheng, X. et al. Ultralight, ultrastiff mechanical metamaterials. *Science* **344**, 1373–1377 (2014).
196. Zheng, X. et al. Multiscale metallic metamaterials. *Nat. Mater.* **15**, 1100–1106 (2016).
197. ProJet 7000 HD. *3D Systems*. https://www.3dsystems.com/3d-printers/projet-7000-hd (2012).
198. Nanoscribe Photonic Professional GT datasheet. https://www.nanoscribe.com (2014).
199. Bückmann, T., Thiel, M., Kadic, M., Schittny, R. & Wegener, M. An elasto-mechanical unfeelability cloak made of pentamode metamaterials. *Nat. Commun.* **5**, 4130 (2014).
200. Yan, W., Cumming, B. P. & Gu, M. High-throughput fabrication of micrometer-sized compound parabolic mirror arrays by using parallel laser direct-write processing. *J. Opt.* **17**, 075803 (2015).
201. EOS P 770 with PA 2200 Top Speed 1.0 datasheet and vendor information. https://www.eos.info (2016).
202. EOS P 110 with PA 2200 Top Quality 1.0 datasheet and vendor information. https://www.eos.info (2016).
203. Pearre, B. W., Michas, C., Tsang, J.-M., Gardner, T. J. & Otchy, T. M. Fast micron-scale 3D printing with a resonant-scanning two-photon microscope. *Addit. Manuf.* **30**, 100887 (2019).
204. Maibohm, C. et al. Multi-beam two-photon polymerization for fast large area 3D periodic structure fabrication for bioapplications. *Sci. Rep.* https://doi.org/10.1038/s41598-020-64955-9 (2020).
205. Stüwe, L. et al. Continuous volumetric 3D printing: xolography in flow. *Adv. Mater.* **11**, e2036716 (2023).

Acknowledgements

The authors thank V. Hahn for the valuable discussions. The authors acknowledge support by the Deutsche Forschungsgemeinschaft (DFG, German Research Foundation) via

the Excellence Cluster "3D Matter Made to Order", EXC-2082/1-390761711, by the Carl Zeiss Foundation through the "Carl-Zeiss-Foundation-Focus@HEiKA", by the Helmholtz Association via the program "Materials Systems Engineering", by the Karlsruhe School of Optics & Photonics (KSOP) at KIT and by the Max Planck School of Photonics (MPSP). X.X. acknowledges the support by the US National Science Foundation (CMMI-2135585). S.M. acknowledges the support by JST CREST JPMJCR1905.

Author contributions

M.W. and P.S. wrote the first draft. P.S. and A.M. arranged the figures. All authors contributed to the writing of all parts of the review.

Competing interests

The authors declare no competing interests.

Additional information

Peer review information *Nature Reviews Physics* thanks Saulius Juodkazis and the other, anonymous, reviewer(s) for their contribution to the peer review of this work.